Title

Bi-allelic variants in OGDHL cause a neurodevelopmental spectrum disease featuring epilepsy, hearing loss, visual impairment, and ataxia

Journal

American Journal of Human Genetics, 108(12)

ISSN

0002-9297

Authors

Yap, Zheng Yie
Efthymiou, Stephanie
Seiffert, Simone
et al.

Publication Date

2021-12-01

DOI

10.1016/j.ajhg.2021.11.003

Peer reviewed

ARTICLE

Bi-allelic variants in *OGDHL* cause a neurodevelopmental spectrum disease featuring epilepsy, hearing loss, visual impairment, and ataxia

Zheng Yie Yap,[1,36] Stephanie Efthymiou,[2,36] Simone Seiffert,[3,36] Karen Vargas Parra,[1] Sukyeong Lee,[4] Alessia Nasca,[5] Reza Maroofian,[2] Isabelle Schrauwen,[6] Manuela Pendziwiat,[7] Sunhee Jung,[8] Elizabeth Bhoj,[9,10] Pasquale Striano,[11,12] Kshitij Mankad,[13] Barbara Vona,[14] Sanmati Cuddapah,[9,10] Anja Wagner,[15] Javeria Raza Alvi,[16] Elham Davoudi-Dehaghani,[17] Mohammad-Sadegh Fallah,[18] Srinitya Gannavarapu,[19] Costanza Lamperti,[5] Andrea Legati,[5] Bibi Nazia Murtaza,[20] Muhammad Shahid Nadeem,[21] Mujaddad Ur Rehman,[22] Kolsoum Saeidi,[23] Vincenzo Salpietro,[11,12] Sarah von Spiczak,[7,24] Abigail Sandoval,[1] Sirous Zeinali,[17] Massimo Zeviani,[25] Adi Reich,[26] SYNaPS Study Group,[2] University of Washington Center for Mendelian Genomics,[27] Cholsoon Jang,[8] Ingo Helbig,[7,28,29,30,31] Tahsin Stefan Barakat,[32] Daniele Ghezzi,[5,33] Suzanne M. Leal,[6,34] Yvonne Weber,[3,35] Henry Houlden,[2] and Wan Hee Yoon[1,*]

Summary

The 2-oxoglutarate dehydrogenase-like (OGDHL) protein is a rate-limiting enzyme in the Krebs cycle that plays a pivotal role in mitochondrial metabolism. *OGDHL* expression is restricted mainly to the brain in humans. Here, we report nine individuals from eight unrelated families carrying bi-allelic variants in *OGDHL* with a range of neurological and neurodevelopmental phenotypes including epilepsy, hearing loss, visual impairment, gait ataxia, microcephaly, and hypoplastic corpus callosum. The variants include three homozygous missense variants (p.Pro852Ala, p.Arg244Trp, and p.Arg299Gly), three compound heterozygous single-nucleotide variants (p.Arg673Gln/p.Val488Val, p.Phe734Ser/p.Ala327Val, and p.Trp220Cys/p.Asp491Val), one homozygous frameshift variant (p.Cys553Leufs*16), and one homozygous stop-gain variant (p.Arg440Ter). To support the pathogenicity of the variants, we developed a novel CRISPR-Cas9-mediated tissue-specific knockout with cDNA rescue system for *dOgdh,* the *Drosophila* ortholog of human *OGDHL*. Pan-neuronal knockout of *dOgdh* led to developmental lethality as well as defects in Krebs cycle metabolism, which was fully rescued by expression of wild-type *dOgdh*. Studies using the *Drosophila* system indicate that p.Arg673Gln, p.Phe734Ser, and p.Arg299Gly are severe loss-of-function alleles, leading to developmental lethality, whereas p.Pro852Ala, p.Ala327Val, p.Trp220Cys, p.Asp491Val, and p.Arg244Trp are hypomorphic alleles, causing behavioral defects. Transcript analysis from fibroblasts obtained from the individual carrying the synonymous variant (c.1464T>C [p.Val488Val]) in family 2 showed that the synonymous variant affects splicing of exon 11 in *OGDHL*. Human neuronal cells with *OGDHL* knockout exhibited defects in mitochondrial respiration, indicating the essential role of *OGDHL* in mitochondrial metabolism in humans. Together, our data establish that the bi-allelic variants in *OGDHL* are pathogenic, leading to a Mendelian neurodevelopmental disease in humans.

[1]Aging and Metabolism Research Program, Oklahoma Medical Research Foundation, Oklahoma City, OK 73104, USA; [2]Department of Neuromuscular Disorders, UCL Queen Square Institute of Neurology, London WC1N 3BG, UK; [3]Department of Neurology and Epileptology, Hertie-Institute for Clinical Brain Research, University of Tübingen, Tübingen 72076, Germany; [4]Verna and Marrs McLean Department of Biochemistry and Molecular Biology, Baylor College of Medicine, Houston, TX 77030, USA; [5]Unit of Medical Genetics and Neurogenetics, Fondazione IRCCS Istituto Neurologico "Carlo Besta," via Temolo 4, 20126 Milan, Italy; [6]Center for Statistical Genetics, Gertrude H. Sergievsky Center, and the Department of Neurology, Columbia University Medical Center, New York, NY 10032, USA; [7]Institute of Clinical Molecular Biology, Christian-Albrechts-University of Kiel, Kiel 24105, Germany; [8]Department of Biological Chemistry, University of California, Irvine, Irvine, CA 92697, USA; [9]Division of Human Genetics, Children's Hospital of Philadelphia, Philadelphia, PA 19104, USA; [10]Department of Pediatrics, Perelman School of Medicine at the University of Pennsylvania, Philadelphia, PA 19104, USA; [11]Department of Neurosciences, Rehabilitation, Ophthalmology, Genetics, Maternal and Child Health, University of Genoa, 16124 Genoa, Italy; [12]Pediatric Neurology and Muscular Diseases Unit, IRCCS, Istituto "Giannina Gaslini," Genoa 16123, Italy; [13]Neuroradiology Unit, Great Ormond Street Hospital for Children, London WC1N3JH, UK; [14]Department of Otolaryngology-Head and Neck Surgery, Tübingen Hearing Research Center, Eberhard Karls University, 72076 Tübingen, Germany; [15]Department of Clinical Genetics, Erasmus University Medical Center, Erasmus MC Cancer Institute, 3000 Rotterdam, the Netherlands; [16]Department of Pediatric Neurology, Institute of Child Health, Children Hospital Lahore, Lahore 54600, Pakistan; [17]Department of Molecular Medicine, Biotechnology Research Center, Pasteur Institute of Iran, Tehran 1316943551, Iran; [18]Department of Medical Genetics, Kawsar Human Genetics Research Center, Tehran 15956-45513, Iran; [19]Department of Pathology and Laboratory Medicine, Western University, London, ON N6A 5C1, Canada; [20]Department of Zoology, Abbottabad University of Science and Technology, Abbottabad 22500, Pakistan; [21]Department of Biochemistry, King Abdulaziz University, Jeddah 21589, Saudi Arabia; [22]Department of Microbiology, Abbottabad University of Science and Technology, Abbottabad 22500, Pakistan; [23]Neuroscience Research Center, Institute of Neuropharmacology, Kerman University of Medical Sciences, Kerman 7616914115, Iran; [24]DRK-Northern German Epilepsy Centre for Children and Adolescents, 24223 Schwentinental-Raisdorf, Germany; [25]Department of Neurosciences, University of Padova, via Giustiniani 2, Padova 35128, Italy; [26]GeneDx, Gaithersburg, MD 20877, USA; [27]University of Washington, Seattle, WA 98195, USA; [28]Division of Neurology, Children's Hospital of Philadelphia, Philadelphia, PA 19104, USA; [29]The Epilepsy NeuroGenetics Initiative, Children's Hospital of Philadelphia, Philadelphia, PA 19104, USA; [30]Department of Biomedical and Health Informatics, Children's Hospital of Philadelphia, Philadelphia, PA 19104, USA; [31]Department of Neurology, University of Pennsylvania, Perelman School of Medicine, Philadelphia, PA 19104, USA; [32]Department of Clinical Genetics, Erasmus University Medical Center, 3015 Rotterdam, the Netherlands; [33]Department of Pathophysiology and Transplantation, University of Milan, 20122 Milan, Italy; [34]Taub Institute for Alzheimer Disease and the Aging Brain, Columbia University Medical Center, New York, NY 10032, USA; [35]Department of Epileptology and Neurology, University of Aachen, Aachen 52074, Germany
[36]These authors contributed equally
*Correspondence: wanhee-yoon@omrf.org
https://doi.org/10.1016/j.ajhg.2021.11.003.

Introduction

The Krebs cycle, also known as the tricarboxylic acid (TCA) cycle, plays an essential role in mitochondrial metabolism in all metazoans. Pathogenic variation in genes encoding enzymes or subunits of enzyme complexes of the Krebs cycle causes recessive neurometabolic diseases. These diseases and the genes that underlie their etiology include Leigh syndrome or Leigh-like disease (*DLD* [MIM: 238331], *SUCLG1* [MIM: 611224], *SUCLA2* [MIM: 603921], *SDHA* [MIM: 600857], and *FH* [MIM: 136850][1–5]), infantile cerebellar-retinal degeneration (*ACO2* [MIM: 100850][6]), infantile leukoencephalopathy (*SDHAF1* [MIM: 612848][7]), and a specific subtype of developmental and epileptic encephalopathy (*MDH2* [MIM: 154100][8]). These diseases are characterized developmental delay and neurological manifestations that include seizures, ataxia, optic atrophy, and encephalopathy. Onset is typically in infancy.

All Krebs cycle enzymes and subunits of enzyme complexes have a single copy of genes in humans but not the genes encoding the enzymes having 2-oxoglutarate dehydrogenase (OGDH) activity for the α-ketoglutarate dehydrogenase complex. *OGDH* (MIM: 613022) and *OGDH*-like (*OGDHL*) (MIM: 617513) appear to have evolved by duplication of a single ancestral gene.[9] OGDH and OGDHL play an essential part in a rate-limiting enzymatic reaction for the conversion of α-ketoglutarate (α-KG) to succinyl-CoA. Similar to other Krebs cycle enzymes, OGDH is widely expressed in most tissues.[10,11] Two individuals carrying a homozygous missense variant in *OGDH* (GenBank: NM_002541.3; c.959A>G [p.Asn320Ser]) presented with developmental delay, seizure, and ataxia.[12] In contrast to the ubiquitous expression of *OGDH*, *OGDHL* expression is mainly restricted to the brain.[11,13] Higher expression of *OGDHL* in human brains suggests the involvement of *OGDHL* in brain development and function.

Here, we report nine individuals from eight unrelated families with bi-allelic variants in *OGDHL*. The individuals presented with diverse neurodevelopmental phenotypes including epileptic encephalopathy, gait ataxia, hearing loss, and optic atrophy, combined with microcephaly and hypoplastic corpus callosum. Functional studies in *Drosophila melanogaster* and fibroblasts showed that all nine single-nucleotide variants (SNVs) identified from individuals carrying bi-allelic *OGDHL* variants are loss-of-function (LOF) alleles, indicating that loss of *OGDHL* function underlies a neurodevelopmental disease in humans.

Subjects and methods

Subjects

Clinical ascertainment included physical examination, medical history interviews, and specialized consultation by pediatric neurologists and clinical geneticists. This study was approved by local institutional review board (IRB)/ethical review boards, and written informed consent was obtained prior to genetic testing from the families involved. Clinical details were obtained through medical file review and clinical examination. Family 1 provided consent according to the protocol of Columbia University (IRB-AAAS2343) approved by the IRB at Columbia University. Family 2 provided consent according to the protocol (ethics committee [EC] reference #21, 9/9/15, Project MitMed) approved by the IRB at University of Milan. Family 3 provided consent according to the IRB protocol (A115/02, A116/02) at the University of Kiel. Family 4 was consented for the research in accordance with IRB-approved protocol (15-012226) of the Epilepsy Genetics Research Project (EGRP) at Children's Hospital of Philadelphia. Families 5, 6, 7, and 8 were consented to the research in accordance with IRB-approved protocol (research ethics committee [REC] reference number: 07/Q0512/26; University College London Hospital [UCLH] project ID number: 07/N018) of University College London.

Exome and Sanger sequencing

DNA was extracted from venous blood according to standard procedures. Exome sequencing (ES) was performed on genomic DNA. We performed ES on a DNA sample from individual 1 from family 1 by using libraries prepared with the NimblegenV2 library preparation kit (Roche, Basel, Switzerland), following the manufacturer's protocol. Sequencing was performed by 100 bp paired-end sequencing on a HiSeq2500 instrument (Illumina, San Diego, California, USA) with a mean on-target coverage of 50×. Filtered reads were aligned to the human genome (Hg19/GRC37) via the Burrows-Wheeler transform method (BWA-MEM). Reads were sorted, and PCR duplicates were marked with Picard. Base quality recalibration and insertion/deletion (InDel) realignments were performed with the Genome Analysis Toolkit (GATK). SNVs and InDel variants were called jointly with HaplotypeCaller and recalibrated with GATK. Annotation and filtering were performed with ANNOVAR and custom scripts. Homozygous and potentially compound heterozygous variants with a population-specific minor allele frequency (MAF) < 0.005 in the Genome Aggregation Database (gnomAD) were selected and prioritized on the basis of their annotation. For the affected probands of family 2, ES was performed as described before.[14] For the affected proband of family 3, ES was performed with Nextera Rapid Capture Expanded Exome Enrichment Kit.[15] For family 4, a duo-ES analysis was performed with genomic DNA from the proband and mother. The exonic regions and flanking splice junctions of the genome were captured the Clinical Research Exome kit (Agilent Technologies, Santa Clara, CA). Massively parallel (NextGen) sequencing was done on an Illumina system with 100 bp or greater paired-end reads. Reads were aligned to human genome build GRCh37/UCSC hg19 and analyzed for sequence variants with a custom-developed analysis tool. Additional sequencing technology and variant interpretation protocol has been previously described.[16] For families 5, 7, and 8, exome sequencing and data analysis were performed as previously described.[17,18] For family 6, exome-coding DNA was captured with the Agilent SureSelect Clinical Research Exome (CRE) kit (v2) and sequenced on an Illumina HiSeq 4000 with 150 bp paired-end reads as described before.[19] The candidate variants were confirmed and segregation analysis was performed with traditional Sanger sequencing for families 1, 2, 3, 5, and 8 (Figure S1, supplemental information). For family 6, trio-whole-exome sequencing was performed at diagnostics.

3D modeling of protein structure

Two homology models were generated with the atomic coordinates of alpha-ketoglutarate decarboxylase (PDB: 2XT6, 2JGD) as

input into Modeler.[20] We combined two models to maximize the predicted ordered region. The final dimer model includes TPP (thiamine pyrophosphate) and magnesium derived from the coordinates of *Mycobacterium smegmatis* alpha-ketoglutarate decarboxylase (PDB: 2XYT).

Cloning and transgenesis

pUASTattB-dOgdh^{P867A}-FLAG, pUASTattB-dOgdh^{R688Q}-FLAG, pUASTattB-dOgdh^{F749S}-FLAG, pUASTattB-dOgdh^{A343V}-FLAG, pUASTattB-dOgdh^{W237C}-FLAG, pUASTattB-dOgdh^{D507V}-FLAG, pUASTattB-dOgdh^{R261W}-FLAG, and pUASTattB-dOgdh^{R316G}-FLAG were generated by site-directed mutagenesis PCR with pUASTattB-dOgdh (WT)-FLAG DNA construct as a template.[21] The primers are listed in Table S3 (supplemental information). A series of pUASTattB-mutant dOgdh constructs were injected into *y,w,ΦC31; VK37* embryos,[22,23] and transgenic flies were selected.

The plasmid pCFD3.1-w-dU:3gRNA-dOgdh was cloned as follows. pCFD3.1-w-dU6:3gRNA was a gift from Simon Bullock (Addgene plasmid # 123366; RRID: Addgene_123366). We phosphorylated, annealed, and cloned 20 bp oligonucleotides containing guide RNA (gRNA) targeting *dOgdh* genomic locus with 4 nt overhangs for BbsI site, into the BbsI site of the pCFD3.1-w-dU:3gRNA vector. The oligonucleotide sequences used for dOgdh gRNA are dOgdh gRNA-F: 5′-GTCG AGGGATACTTACGGTGTG CA-3′ and gRNA-R: 5′-AAAC TGCACACCGTAAGTATCCCT-3′. The pCFD3.1-w-dU:3-gRNA^{dOgdh} construct was injected into *y,w,ΦC31; P{CaryP}attP40* embryos, and transgenic flies were selected.

Fly strains and maintenance

The following stocks were obtained from the Bloomington *Drosophila* Stock Center at Indiana University (BDSC): *elav^{C155}-Gal4*, *elav^{C155}-Gal4*; *UAS-Cas9.P2* (on III). All flies were maintained at room temperature (21°C) and crosses were kept at 25°C.

Immunoblot

Fly heads were homogenized in 1× Laemmli sample buffer containing 2.5% β-mercaptoethanol with pellet pestles (Sigma-Aldrich). After boiling for 10 min, samples were briefly centrifuged. Supernatants loaded into 4%–20% Mini-PROTEAN TGX Stain-Free Protein Gels (Bio-Rad), separated by SDS-PAGE, and transferred to nitrocellulose membranes (Bio-Rad). The primary antibodies were used for overnight shaking at 4°C by the following dilution: mouse anti-FLAG M2 (Sigma Cat# F1804 RRID: AB_262044) 1:1,000; rabbit anti-OGDHL (Proteintech Cat# 17110-1-AP) 1:1,000; rabbit anti-OGDH (Abcam Cat# ab137773) 1:1,000; mouse anti-Actin (MP Biomedicals Cat# 8691002). HRP-conjugated goat anti-mouse (Thermo Fisher Scientific Cat# A-28177 RRID: AB_2536163) and goat anti-rabbit antibodies (Thermo Fisher Scientific Cat# A10547 RRID: AB_2534046) were used at 1:7,000 and visualized with enhanced chemiluminescence (ECL) (Bio-Rad).

Drosophila bang sensitivity assay

Methods were adapted from Howlett et al., 2013.[24] Briefly, 20 flies were anesthetized with CO_2 and were allowed to rest in fresh food vials for 24 h at 25°C before the assay. The male and female flies used were maintained at 1:1 ratio so there would be less chance of gender differences. On the day of the assay, flies were transferred into empty polystyrene vials without the use of CO_2 and left to acclimatize to the surrounding for 15 min. They were then vortexed (Vortex-Genie 2 Scientific Industries) for 10 s at maximum strength.[25] For data analysis, we recorded a 40 s video to measure the number of flies able to recover and climb at each time point. Five trials were conducted (n ≈ 100 for each genotype).

cDNA analysis

Fibroblasts from individual 3 and two age-matched controls (without any rare variant in *OGDHL*) were grown in DMEM supplemented with 1 mM pyruvate, 4.5 g/L glucose, 10% fetal calf serum, and 1% penicillin/streptomycin at 37°C in 5% CO_2. For RNA purification from fibroblasts and cDNA retrotranscription, we used RNeasy mini kit (QIAGEN) and GoTaq 2-Step RT-qPCR System (Promega), respectively, according to the manufacturer's protocols. For *OGDHL* cDNA amplification (GenBank: NM_018245.3), we used the following primer pair: 589F/2413R (589F: 5′-TGGAGAACACCTACTGCCAG-3′; 2413R: 5′-CCTCGAA GTCCTTGGTGAATG-3′). For sequencing of *OGDHL* transcript, PCR products were processed with Nextera XT DNA sample preparation kit (Illumina). Next-generation sequencing (NGS) was performed on an Illumina MiSeq instrument and reads were then aligned with BWA and visualized with Integrating Genomics Viewer (IGV).

Metabolite analysis with liquid chromatography/mass spectrometry (LC/MS)

Metabolites in brain tissues were extracted by 45 μL of ice-cold acetonitrile:methanol:water (40:40:20) solution containing 0.5% formic acid. We added 4 μL of 15% NH_4HCO_3 (w/v) in acetonitrile: methanol:water (40:40:20) solution to neutralize pH. Following vortexing and centrifugation at 16,000 g for 10 min at 4°C, extract was loaded to individual vials. Metabolites were analyzed by quadrupole-orbitrap mass spectrometers (Q-Exactive Plus Hybrid Quadrupole-Orbitrap, Thermo Fisher Scientific) coupled to hydrophilic interaction chromatography (HILIC) via electrospray ionization. Liquid chromatography (LC) separation was performed on an Xbridge BEH amide column (2.1 mm × 150 mm, 2.5 μm particle size, 130 Å pore size; waters) at 25°C with a gradient of solvent A (5% acetonitrile in water with 20 mM ammonium acetate and 20 mM ammonium hydroxide) and solvent B (100% acetonitrile). Flow rate was 350 μL/min. The LC gradient was as follows: 0 min, 75% B; 3 min, 75% B; 4 min, 50% B; 5 min, 10% B; 7 min, 10% B; 7.5 min, 75% B; 11 min, 75% B. Autosampler temperature was set at 4°C and the injection volume of the sample was 5 μL. Mass spectrometry (MS) analyses were acquired in negative ion mode with MS full-scan mode from m/z 70 to 830 and 140,000 resolution. Data analysis was performed with MAVEN software.

OGDHL knockout human neuronal cells

Creation of *OGDHL* knockout SH-SY5Y cell was performed as previously described.[26,27] Briefly, we selected two guide RNAs targeting the exon 2 genomic region of human *OGDHL* with high activity and minimum off-target by using Synthego prediction tools. Then, we cloned double-strand DNA fragments for gRNA1^{OGDHL} (5′-GCCTGTACCCCAAGACGGGA-3′), gRNA2^{OGDHL} (5′-TCGCAG CCTGTACCCCAAGA-3′), and scramble (control) (5′-GCACTAC CAGAGCTAACTCA-3′) into LentiCRISPRv2 vector. By transfecting these vectors into HEK293T, we generated lentiviruses, which we used for transduction of SH-SY5Y cells with puromycin selection. *OGDHL* knockout were confirmed by immunoblot and ICE (inference of CRISPR edits) analysis (Synthego Performance Analysis, ICE Analysis. 2019. v2.0. Synthego; [6.11.2021]).

Cellular respiration assay

We used XFe24 analyzer from Seahorse Biosciences to measure the rate of oxygen consumption, according to the manufacture's protocol. Briefly, control and *OGDHL* knockout cells were seeded at a density of 8×10^4 cells per each well of a XFe24 cell culture plate (Agilent 100777-004). The next day, the cells were pre-incubated for 1 h with complete XF DMEM (Agilent 103575-100) containing 10 mM glucose, 1 mM sodium pyruvate, and 2mM L-glutamine. We used the complete XF DMEM to prepare cellular stress reagents to provide the following final concentration: 1 μM oligomycin, 1 μM FCCP (Carbonyl cyanide 4-(trifluoromethoxy)phenylhydrazone), and 1 uM antimycin A. All the reagents were loaded in the ports in cartridge unit. Oxygen consumption rates were measured for 3 min for mixing and 2 min of waiting period. Basal respiration was calculated by subtracting non-mitochondrial respiration rate from last rate measurement before oligomycin injection. Maximal respiration was calculated by subtracting non-mitochondrial respiration rate from maximum rate measurement after FCCP injection. We calculated ATP production by subtracting minimum rate measurement after oligomycin injection from last rate measurement before oligomycin injection.

Results

Clinical findings

We identified nine individuals from eight families carrying bi-allelic variants in the *OGDHL* gene through whole-exome sequencing (WES) (Figure 1A). All groups were connected to study the *OGDHL* gene through GeneMatcher.[28,29] For recruiting individual 7, we have contacted close collaborators from genomic centers in Europe and the USA. Parental consanguinity was reported in five of the eight families (families 1, 5, 6, 7, and 8), all of whom had homozygous variants in *OGDHL* (Figure 1A). The remaining three individuals showed compound heterozygous variants (families 2, 3, and 4). The clinical features of the affected individuals are summarized in Tables 1 and S1 and are described further in the supplemental notes.

The individuals presented between 2 months and 8 years with a median onset of 1.9 years. Eight of nine individuals presented with mild to severe developmental delay. Feeding difficulties in four individuals (3, 5, 6, and 8) were noted, and excessive laughing/crying was observed in individual 8. Six individuals (individuals 1, 3, 5, 6, 8, and 9) showed an ophthalmological involvement that included visual impairment, nystagmus, and optic atrophy. Profound bilateral sensorineural hearing loss was found in four individuals (individuals 1, 2, 3, and 9). Dysmorphic features were reported in five of nine individuals (individuals 3, 4, 5, 6, 7, and 9) mainly consisting of distinctive craniofacial features including highly arched palate, bilateral ptosis, and downward slanting of eyes (Figures 2E and 2F). Neurological examination showed gait ataxia, spasticity, neuropathy, and hypotonia in seven individuals (individuals 1, 2, 3, 5, 6, 8, and 9). Five individuals (1, 4, 5, 6, and 9) experienced seizures at least once in their life with variable presentations (absences-, tonic-, tonic-clonic-, myoclonic-atonic-, atonic-, focal motor seizures, and infantile spasms). In addition, one person (individual 4) showed a severe obtundation status. Electroencephalogram (EEG) for individuals 5, 6, and 9 were available, and their EEGs were variable with generalized multifocal slowing intermixed with multi-focal sharp discharge (Figures S2–S4). This could be suggestive of a severe bilateral cerebral dysfunction with multi-focal and generalized epileptiform potential, consistent with a transition from infantile spasms to Lennox-Gastaut Syndrome. Brain MRI was available in four individuals (individuals 3, 6, 7, and 9) (Figures 2A–2D). A diverse spectrum of abnormalities was observed on neuroimaging. Individual 6 in family 5 presented with microcephaly (<3rd percentile of head circumference from age 6.5 to 8.5 years). MRI scan on individual 6 in family 5 showed a slender corpus callosum (Figure 2A3), which is similar to those in the previously identified person carrying a homozygous p.Ser778Leu variant.[21,30] Frank basal ganglia cavitating damage and cystic leukomalacia was present in individual 6 (Figure 2A). Signal abnormality was noted in the small brain stem nuclei in both individual 6 (family 5) and individual 3 (family 2) (Figures 2A and 2B). The MRI scan on individual 7 in family 6 revealed a low-grade neoplasm with no additional findings (Figure 2C), and the imaging on individual 9 in family 8 showed subtle cortical dysgyria (Figure 2D).

In summary, our individuals with bi-allelic *OGDHL* variants display a broad spectrum of neurological features including epilepsy, gait ataxia, hearing loss, visual impairment, malformations of cortical development, microcephaly, hypoplastic corpus callosum, and dysmorphic signs.

Genetic findings

WES in the affected probands revealed 11 novel bi-allelic variants in *OGDHL* (Figure 1, Table S2, supplemental information). Five of the identified variants were homozygous: three missense variants (c.2554C>G [p.Pro852Ala] in individuals 1 and 2 [family 1]; c.730C>T [p.Arg244Trp] in individual 6 [family 5]; c.895A>G [p.Arg299Gly] in individual 8 [family 7]), a frameshift variant (c.1658delG [p.Cys553Leufs*16] in individual 7 [family 6]), and a stop-gain variant (c.1318C>T [p.Arg440Ter] in individual 9 [family 8]). Three individuals from families 2, 3, and 4 carry compound heterozygous single-nucleotide variants (SNVs): c.2018G>A (p.Arg673Gln)/c.1464T>C (p.Val488Val) in individual 3, c.2201T>C (p.Phe734Ser)/c. 980C>T (p.Ala327Val) in individual 4, and c.660G>C (p.Trp220Cys)/c.1472A>T (p.Asp491Val) in individual 5 (Figure 1A). All of the altered residues are evolutionarily conserved across species (Figure 1B). The heterozygous Phe734Ser variant has been previously implicated in eosinophilic esophagitis.[31] The other variants have not been reported previously as pathogenic variants. Variants identified in families 1, 2, 3, and 6 (Pro852Ala, Arg673Gln, Ala327Val, and p.Cys553Leufs*16) were absent in publicly available population databases such as gnomAD, Exome Sequencing Project (ESP), GME Variome, and Iranome, as

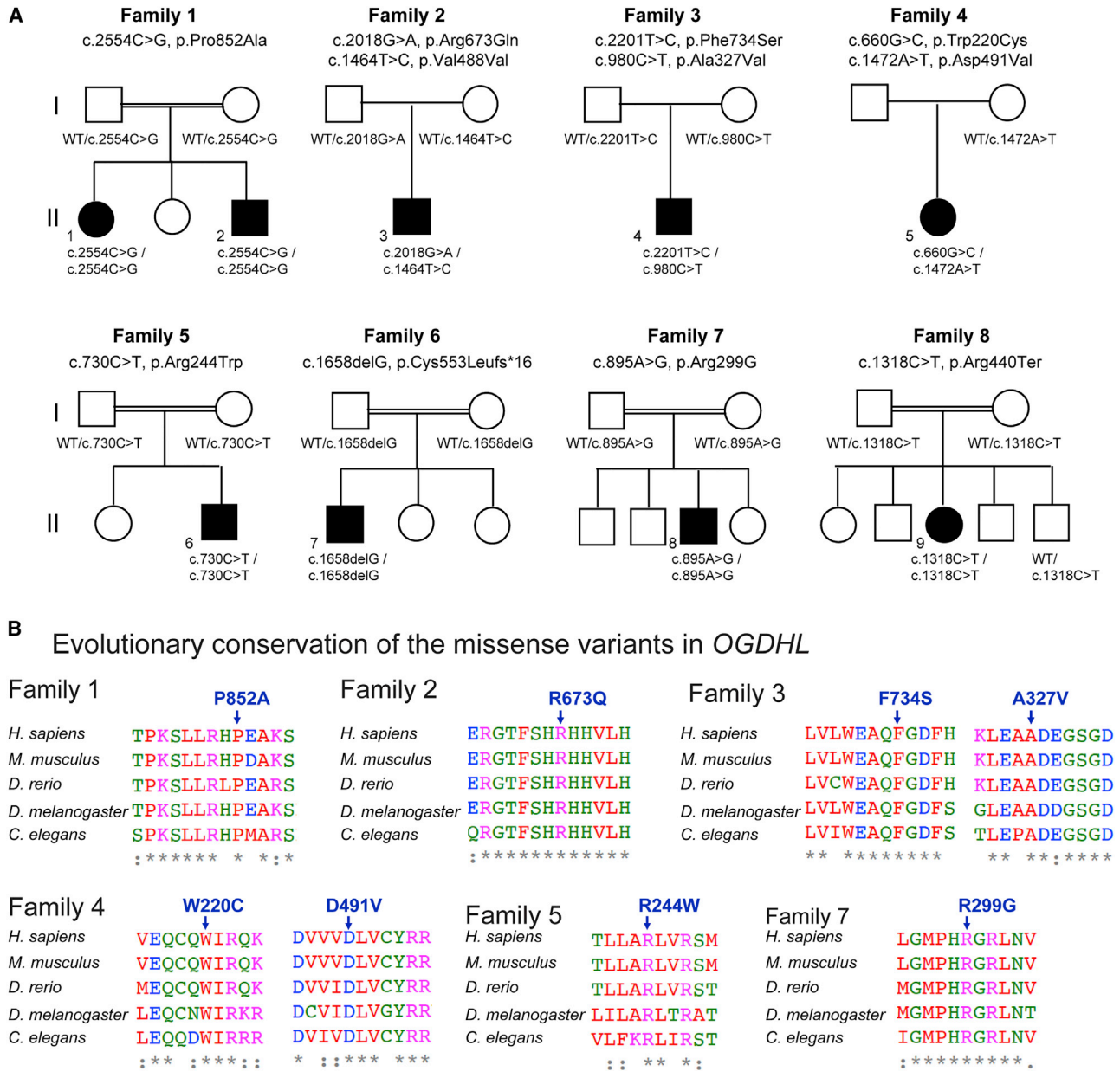

Figure 1. Identification of individuals with neurodevelopmental phenotypes with SNVs in *OGDHL*
(A) Eight pedigrees drawings, indicating bi-allelic variants in *OGDHL* identified in nine individuals from eight families. Homozygous missense variants were identified in families 1, 5, and 7, a homozygous frameshift variant in family 6, a homozygous stop-gain variant in family 8, and compound heterozygous variants in families 2, 3, and 4.
(B) Multiple-sequence alignment confirms evolutionary conservation of the eight missense variants in the animal kingdom.

well as in over 16,000 in-house exomes at Queen Square Genomics, UCL. On the basis of *in silico* predictions, all variants had high CADD scores (Table S2), with an average CADD score of 31.2, and are thus most likely damaging and deleterious variants.

In silico homology modeling and structural analysis of missense variants identified in affected individuals

To generate a homology model for human OGDHL, we used the atomic coordinates for alpha-ketoglutarate decarboxylase as input into Modeler.[20] *In silico* structure model suggested that each variant would alter the predicted protein structure (Figures 3B and 3C). The model showed that OGDHL forms a homodimer in which each subunit binds with a TPP (thiamine pyrophosphate) cofactor to form a substrate-binding pocket for OGDHL (Figure 3C). Importantly, the model shows that the mutated residues from two variants Phe734Ser and Arg299Gly are located in the substrate-binding pocket (Figure 3C). The side chain of Phe734 forms a part of the binding site for the pyrimidine ring and thiazole ring of TPP and contributes to the aromatic side-chain relay including the pyrimidine ring

Table 1. Summary of the clinical and genetic information of the analyzed cohort

	Individual 1 (family 1)	Individual 2 (family 1)	Individual 3 (family 2)	Individual 4 (family 3)	Individual 5 (family 4)	Individual 6 (family 5)	Individual 7 (family 6)	Individual 8 (family 7)	Individual 9 (family 8)	Individual 10 (Yoon et al., 2017[21])
Variant GenBank: NM_018245	c.2554C>G (p.Pro852Ala)	c.2554C>G (p.Pro852Ala)	c.2018G>A (p.Arg673Gln); c.1464T>C (p.Val488Val)	c.2201T>C (p.Phe734Ser); c.980C>T (p.Ala327Val)	c.660G>C (p.Trp220Cys); c.1472A>T (p.Asp491Val)	c.730C>T (p.Arg244Trp)	c.1658delG (p.Cys553Leufs*16)	c.895A>G (p.Arg299Gly)	c.1318C>T (p.Arg440Ter)	c.2333C>T (p.Ser778Leu)
Inheritance	hom.	hom.	com. het.	com. het.	com. het.	hom.	hom.	hom.	hom.	hom.
AoO	birth	1 year	8 years	6 years	6 months	5 months	3 months	3–4 months	2 months	1 year
DD/ID	mild DD	mild DD	mild DD	no	global DD	global DD and ID	mild ID	moderate to severe ID	global DD and ID	severe DD and ID
Seizures (onset)	1X TC	no	no	abs., MA, TC, SE (N/A)	IS, TC (6 months)	focal-motor, TC (2 years)	no	no	yes (12 months)	no
Neurologic examination	mild GA	mild GA	GA, axonal neuropathy, spasticity	normal	hyp., no walking	spastic, quadriplegic, no walking	normal	hyp., walk with help	hyp., GA, walk with help	hyp., hypertonicity, spasticity, GA
EEG features	N/A	N/A	normal	N/A	hypsarrhytmia, multifocal/gen. spikes	diffuse spikes, slowed background activity	N/A	mild slowed background	T-R spikes	N/A
Hearing involvement	profound bi.	profound bi.	profound	no	no	no	no	no	bi. hearing deficit	no
Ophthalmological involvement	VI	no	retinopathy	no	VI, nystagmus	bi. optic atrophy	no	mild nystagmus	poor vision	no
Dys. features	no	no	hypomimia, scoliosis, pes cavus	no	bi. hip dysplasia, clonus with extension of right foot	high arched palate, scoliosis, microcephaly	scaphocephaly	no	bi. ptosis, highly arched palate, down slanting of eyes	some synophrys, large mouth, microcephaly
MRI	N/A	N/A	bi. unspecific T2 lesions	normal	global atrophy, diffuse T2 hyperintens., focus frontal	periv. leukomalacia, corpus callosum hypoplasia	R-F glioma	normal	normal	hypo plastic corpus callosum, global atrophy
Main phenotype	hearing deficit	hearing deficit	dysmorphic features	DEE	DEE	DEE	ID	ID	hearing and vision deficit, DEE	dysmorphic features, ID

abs., absence; AoO, age of onset; bi., bilateral; com. het., compound heterozygous; DD, developmental delay; GA, gait ataxia; hom., homozygous, hyp., hypotonia; hyperintense., hyperintensity; ID, intellectual disability; IS, infantile spasms; MA, myoclonic-atonic; DEE, developmental and epileptic encephalopathy; N/A not available; periv., periventricular; R-F, right frontal; SE, status epilepticus; TC, tonic-clonic; VI, visual impairment.

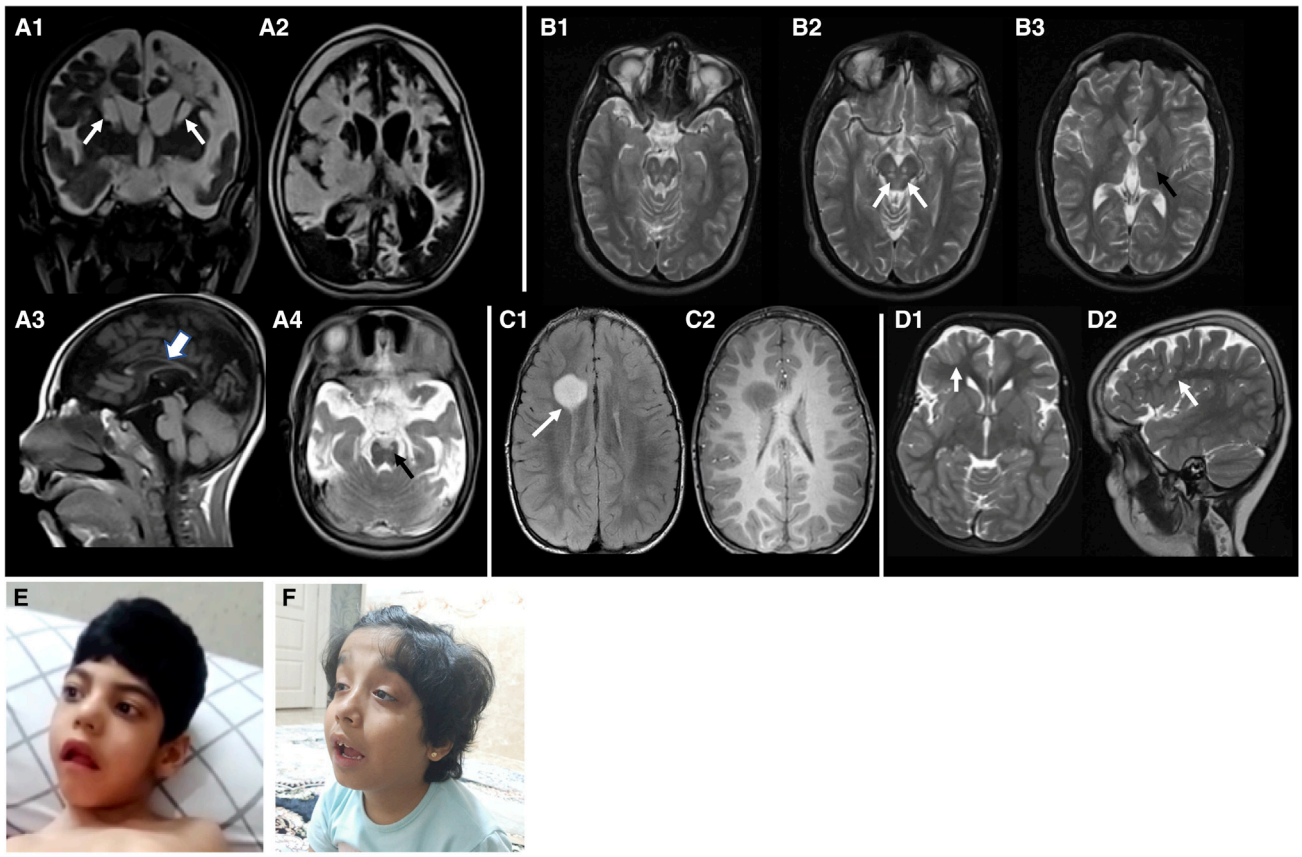

Figure 2. Clinical findings of affected individuals

(A) MRI of family 5 (individual 6). Coronal T2 (A1) and axial FLAIR (A2) scans show extensive scarring involving the white and gray matter structures of the brain with frank cavitation involving the caudate nuclei and the adjacent deep white matter of the cerebral hemispheres (arrows-A1). Sagittal T1 (A3) shows a slender corpus callosum (arrow) and axial T2 (A4) image shows symmetric involvement of brain stem nuclei (black arrow).

(B) MRI of family 2 (individual 3). Axial T2 sections showing symmetric involvement of the brain stem nuclei (arrows-B2) and the thalamo-capsular regions bilaterally (black arrow-B3).

(C) MRI of family 6 (individual 7). Axial FLAIR (C1) and post-contrast T1 (C2) images show a low-grade astrocytoma adjacent to the lateral ventricle on the right (arrow-C1).

(D) MRI of family 8 (individual 9). Axial T2 (D1) and sagittal T2 (D2) images show cortical dysgyria (arrows).

(E) Individual 6 in family 5 presents with microcephaly. He has a highly arched palate. He has no visual interaction but makes roving eye movements.

(F) Individual 9 in family 8 presents with macrocephaly and mild dysmorphic features, including bilateral ptosis, highly arched palate, and eye downslanting.

of TPP. Serine substitution for Phe734 (F734S) would disrupt this interaction. Arg299 forms ionic interaction with the β-phosphate of the bound TPP as shown in Figure 3C. This interaction is critical for TPP binding, thereby Gly substitution for Arg299 (R299G) is predicted to impair the interaction. Hence, the analysis suggests that Phe734Ser and Arg299Gly may lead to substantial defects in OGDHL function.

We examined the other six missense variants, Pro852Ala, Arg673Gln, Asp491Val, Trp220Cys, Arg244Trp, and Ala327Val (Figure 3B). The side chain of Pro852 forms a local aromatic proline interaction. Alanine substitution for proline 852 (Pro852Ala) would abolish this interaction and negatively affect the structural stability. Arg673 forms two ionic interactions with the side chains of Glu644 and Glu731 as well as a hydrogen bond with the main chain carbonyl of Val665. Glutamine substitution for Arg673 (Arg673Gln) is predicted to destabilize the interaction because of the shorter side chain length and lack of a positive charge. The side chain of Asp491 forms hydrogen bonds with side chains of Asn430 and His461 of neighboring β strands, which can contribute to the stability of the β sheet. Thus, aspatate to valine substitution (Asp491Val) would destabilize the β sheet, which also includes the next β strand connected to the helix containing Trp220. Trp220 forms aromatic cluster together with Trp480 and Phe484. Cysteine mutation on Trp220 (Trp220Cys) will abolish the T shape pi network of this aromatic cluster. Arg244Trp substitution would cause losing flexible charged surface residue and adding a rigid bulky tryptophan residue, which may reduce entropy and protein solubility in addition to causing steric clashes with residues in the neighboring helix. Ala327 is surface exposed and the alanine to valine mutation may reduce protein

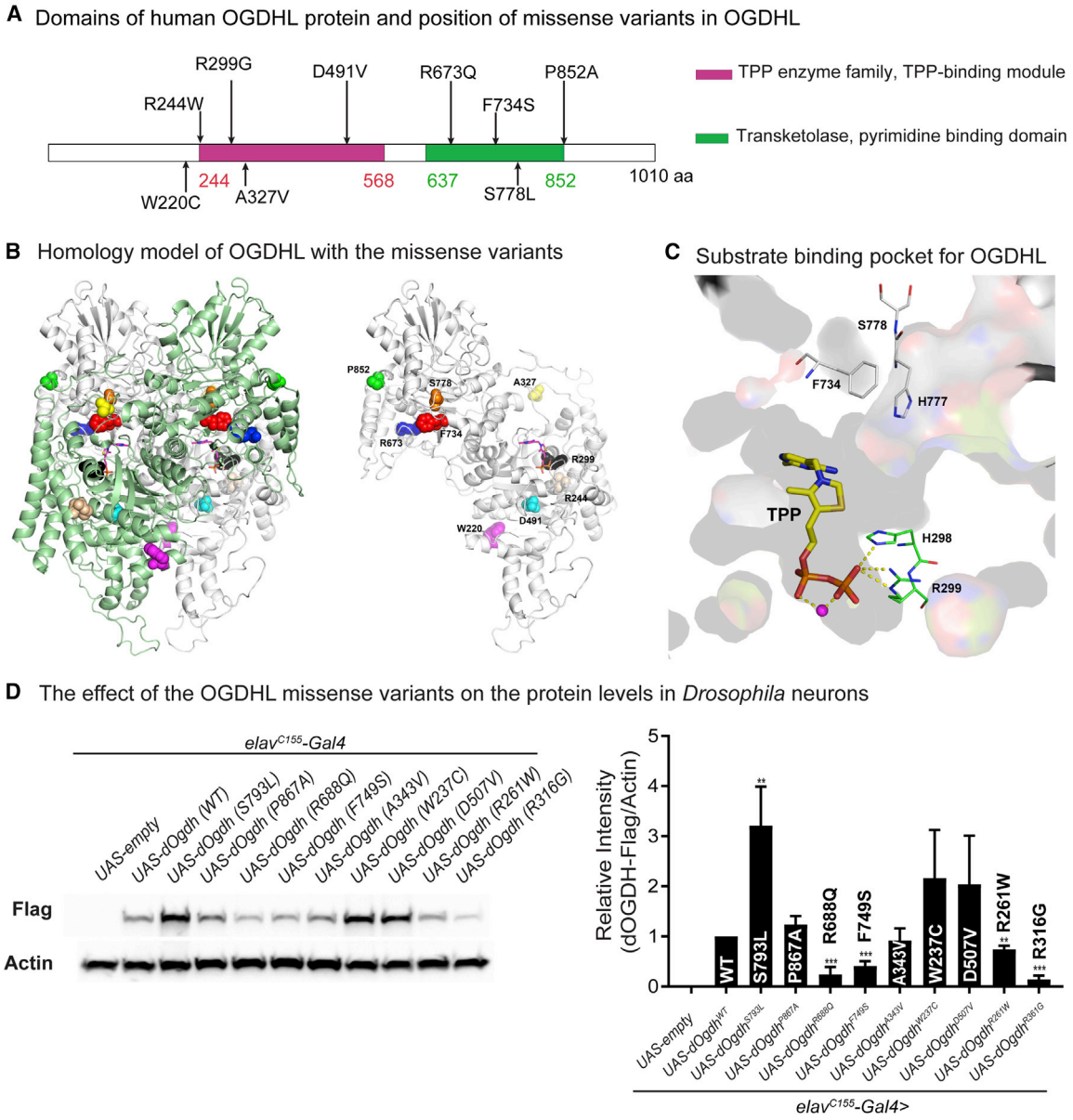

Figure 3. Protein modeling of OGDHL dimer and the effects of eight missense variants on protein levels

(A) Schematic representation of protein domains of human OGDHL and positions of the eight missense variants together with the previously identified p.Ser778Leu variant. Pink indicates a TPP-binding domain. Green indicates a transketolase domain.

(B) *In silico* protein structure prediction of human OGDHL dimer and position of mutated residues. Dimer of OGDHL is shown in ribbon (left). Each monomer is colored with green and white. Bound TPP is shown in stick model and mutation sites are in CPK model. One monomer is shown for clarity (right).

(C) Only thin section of substrate binding pocket was shown with surface rendering for clarity. Amino acid residues involved in missense variants in the pocket are shown in stick model together with TPP. Residues from *cis* subunit are shown in green and residues from *trans* in gray. Bound magnesium is shown in magenta ball.

(D) Immunoblots for *Drosophila* heads expressing wild-type dOgdh-FLAG or dOgdh-FLAG carrying the homologous missense variants identified from individuals with bi-allelic *OGDHL* variants. Three biological replicates were quantified. Error bars represent SEM. p values were obtained by ANOVA. $^{**}p < 0.01$, $^{***}p < 0.001$.

solubility by exposing more hydrophobic side chain to the surface. We also examined the previously identified pathogenic variant Ser778Leu that underlies severe neurodevelopmental defects in humans.[21] We found that Ser778Leu would disturb the surrounding local structure because there is not enough space to accommodate the bulky side chain of leucine, which will affect Pro980 and Thr982, destabilizing the dimer interface. The structural change caused by Ser778Leu mutation would affect the conformation of His777, resulting in disturbance of the aromatic cluster formed by side chains of Phe734 and Phe737, which would negatively affect the binding of Phe737 with the pyrimidine ring of TPP, and dimer formation. Collectively, *in silico* analyses suggest that all these

A Expression of *dOgdh* cDNAs by *dOgdh-T2A-Gal4*

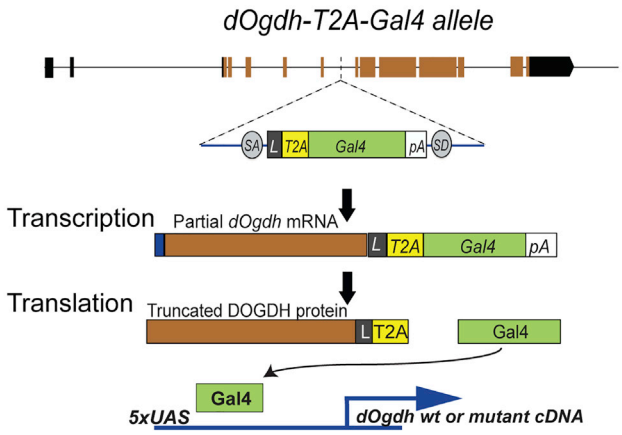

B Missense variants in human OGDHL and dOgdh

***Hs* OGDHL**	S778L	P852A	R673Q	F734S	A327V	W220C	D491V	R244W	R299G
***Dm* OGDH**	S793L	P867A	R688Q	F749S	A343V	W237C	D507V	R261W	R316G

C Functional test for 8 new *OGDHL* variants using *dOgdh-T2A-Gal4* allele

Genotypes	Rescue of lethality
dOgdh−T2A−Gal4 / *dOgdh−T2A−Gal4*	Lethal
UAS-dOgdh(WT)-Flag; dOgdh−T2A−Gal4	Rescue Lethality
UAS-dOgdh(S793L)-Flag; dOgdh−T2A−Gal4	Lethal
UAS-dOgdh(P867A)-Flag; dOgdh−T2A−Gal4	Lethal
UAS-dOgdh(R688Q)-Flag; dOgdh−T2A−Gal4	Lethal
UAS-dOgdh(F749S)-Flag; dOgdh−T2A−Gal4	Lethal
UAS-dOgdh(A343V)-Flag; dOgdh−T2A−Gal4	Lethal
UAS-dOgdh(W237C)-Flag; dOgdh−T2A−Gal4	Lethal
UAS-dOgdh(D507V)-Flag; dOgdh−T2A−Gal4	Lethal
UAS-dOgdh(R261W)-Flag; dOgdh−T2A−Gal4	Lethal
UAS-dOgdh(R316G)-Flag; dOgdh−T2A−Gal4	Lethal

Figure 4. Functional studies for OGDHL missense variants with *dOgdh*-null mutant
(A) Schematic of *dOgdh-T2A-Gal4* allele and the Gal4/UAS system.
(B) The table shows missense variants in *OGDHL* and the *Drosophila Ogdh* variants homologous to the human variants.
(C) The lethality caused by loss of *dOgdh* was rescued by expression of wild-type *dOgdh* but not by those carrying any missense variants homologous to those identified from individuals with bi-allelic *OGDHL* variants.

missense variants identified from individuals carrying bi-allelic *OGDHL* variants could impair OGDHL structure and function.

The effects of the missense variants on protein levels

To determine the effects of a series of missense variants identified from individuals with bi-allelic *OGDHL* variants on *in vivo* protein levels, we generated transgenic flies harboring cDNA of *dOgdh*, the *D. melanogaster* (*Dm*) ortholog of human *OGDHL*, that carry homologous mutations to the human missense variants under the control of upstream activating sequence (UAS) (*UAS-dOgdh*^{P867A}, *UAS-dOgdh*^{R688Q}, *UAS-dOgdh*^{F749S}, *UAS-dOgdh*^{A343V}, *UAS-dOgdh*^{W237C}, *UAS-dOgdh*^{D507V}, *UAS-dOgdh*^{R261W}, and *dOgdh*^{R316G}) (Figure 4B). Using pan-neuronal Gal4 driver (*elav*^{C155}*-Gal4*), we expressed each mutant transgene, wild-type *dOgdh* (*UAS-dOgdh*^{WT}), as well as *Dm* mutation for the pathogenic S778L variant (*UAS-dOgdh*^{S793L})[21] (Figure 3D). All transgenes have C-terminal FLAG for protein analysis. Immunoblot for adult fly heads showed that the variants that are predicted to impair TPP-binding, including *Dm* Arg316Gly (human Arg299Gly) and *Dm* Phe749Ser (human Phe734Ser), caused a substantial decrease in the protein levels (Figure 3D). In addition, we found that the protein levels of *Dm* Arg688Gln (human Arg673Gln) are significantly lower than those in wild-type control, and *Dm* Arg261Trp (human Arg244Trp) caused decreased protein levels in lesser extent (Figure 3D). On the contrary, *Dm* Ser793Leu (human Ser778Leu) led to a significant increase in the protein levels. This suggest that Ser793Leu may lead to misfolded protein aggregates that cannot be degraded by the protein quality control system. The protein levels for *Dm* Pro867Ala (human Pro852Ala), *Dm* Ala343Val (human Ala327Val), *Dm* Trp237Cys (human Trp220Cys), and *Dm* Asp507Val (human Asp491Val) were not significantly different from protein levels in the wild-type control (dOgdh WT) (Figure 3D). Hence, these results suggest that Arg673Gln, Arg299Gly, and Phe734Ser may cause loss of OGDHL function.

In vivo functional studies for the variants in *OGDHL* with *dOgdh*-null mutant flies

We sought to determine the functional effects of the missense variants in *OGDHL*. To this end, in our previous work, we created a loss-of-function mutant for *dOgdh* by insertion of a T2A-Gal4 cassette into the coding intron of *dOgdh* by using recombination-mediated cassette exchange.[21,32,33] The *dOgdh* mutant allele (*dOgdh-T2A-Gal4*) expresses the GAL4 transgene under control of the endogenous cis-regulatory elements of *dOgdh*. The GAL4 protein in turn activates expression of genes downstream of UAS (Figure 4A). We previously showed that loss of *dOgdh* (homozygous for *dOgdh-T2A-Gal4*) caused lethality, which was rescued by expression of wild-type *dOgdh* (*dOgdh*^{WT}) but not by expression of *dOgdh* carrying a homologous mutation to human OGDHL (Ser778Leu) (*dOgdh*^{S793L}).[21] Thus, these results demonstrated that

dOgdh-T2A-Gal4 mutant is a suitable model for functional interpretation of disease candidate variants in human *OGDHL*. Using the *dOgdh-T2A-Gal4* mutants and transgenic flies harboring *UAS-dOgdh* cDNA carrying homologous mutations to new *OGDHL* variants (Figure 4B), we performed the lethality rescue assay. Flies carrying *UAS-dOgdh*^{WT} and *UAS-dOgdh*^{S793L} served as controls for the assay. We found that expression of none of eight new missense variants rescued the lethality caused by *dOgdh* loss (Figure 4C). Thus, the results indicate that all eight missense variants are loss-of-function alleles.

Functional studies for the variants in *OGDHL* in neurons

In humans, *OGDHL* is mainly expressed in the brain, whereas *OGDH* is expressed ubiquitously.[10,13] The single *Dm* ortholog, *dOgdh* for human *OGDHL* and *OGDH*, is ubiquitously expressed in tissues including nervous and muscular systems.[12] Hence, the study from the *dOgdh*-null mutant (*dOgdh-T2A-Gal4*) (Figure 4) would not determine the functional effects of the variants specifically on the nervous system. To determine the effects of the identified variants specifically in the nervous system, we developed a novel CRISPR-Cas9-mediated method for tissue-specific knockout (ko) with cDNA rescue (Figure 5A). The current CRISPR-Cas9 method in the *Drosophila* field permits tissue specificity, but most guide RNAs (gRNAs) target exons and thereby target both genomic loci and cDNA transgenes.[34] As such, the current system prevents rescue of ko phenotypes by cDNA transgene expression. We overcame this technical obstacle by developing a strategy that selectively targets genomic loci but not UAS transgenes by using gRNAs that are complementary to the exon-intron junctions of target genes. Figures 5A and 5B illustrate how we applied this new method to study the functional effects of the *OGDHL* variants on the nervous system. To determine the effect of neuronal ko of *dOgdh*, we generated transgenic flies harboring the gRNA for *dOgdh* (*gRNA*^{dOgdh}) that is ubiquitously expressed by U6:3 promotor and *UAS-Cas9.P2* that is expressed by a pan-neuronal Gal4 (*elav*^{C155}*-Gal4*). Neuronal ko for *dOgdh* (*elav*^{C155}*-Gal4; U6:3-gRNA*^{dOgdh}*/UAS-empty; UAS-Cas9.P2*) resulted in lethality, which was fully rescued by expression of wild-type *dOgdh* cDNA (Figure 5C). By performing Sanger sequencing for fly heads, we demonstrated that gRNA^{dOgdh} and Cas9.P2 efficiently targeted the genomic locus of *dOgdh* but not *dOgdh* cDNA in the UAS transgene (Figure 5B). The expression of the known pathogenic *dOgdh*^{S793L} mutant failed to rescue the lethality caused by neuronal *dOgdh* ko (Figure 5C). Hence, the results demonstrated that our new system enables determining the functional effects of the missense variants in *OGDHL* identified from our cohort in neuronal context.

Unlike the *dOgdh-T2A-Gal4* assay, the CRISPR-Cas9-mediated neuronal ko with cDNA rescue system revealed various allelic strength for eight missense variants. We first found that three missense variants *dOgdh*^{R688Q}, *dOgdh*^{F749S}, and *dOgdh*^{R316G} failed to rescue the developmental lethality caused by neuronal ko of *dOgdh*. The results indicate that these three variants are severe loss-of-function alleles. This result is consistent with our 3D homology model that predicted the important role of the residues in TPP-binding (human Phe734Ser and Arg299Gly) (Figure 3C), as well as reduced protein levels (*Dm* Arg688Gln, *Dm* Phe749Ser, and *Dm* Arg316Gly) (Figure 3D). On the contrary, the other five missense variants, *dOgdh*^{P867A}, *dOgdh*^{A343V}, *dOgdh*^{W237C}, *dOgdh*^{D507V}, and *dOgdh*^{R261W}, rescued the lethality (Figure 5C). We confirmed that the dOgdh proteins with these five missense variants were expressed in adult brains by performing immunoblot (Figure S5). To determine the effects of the five variants in adult stage, we performed bang-sensitivity assay. We found that flies carrying *dOgdh*^{R261W} exhibited a recovery defect from mechanical stress at both day 5 and day 10, whereas flies having the other four variants, *dOgdh*^{P867A}, *dOgdh*^{A343V}, *dOgdh*^{W237C}, or *dOgdh*^{D507V}, did show comparable recovery to wild-type controls at day 5, but exhibited delayed recovery at day 10 (Figure 5D). Hence, the data indicate that Arg261Trp has more defective gene function compared to the other four variants (Pro867Ala, Ala343Val, Trp237Cys, and Asp507Val). Collectively, the results from our new CRISPR-Cas9-mediated neuronal ko system indicate that three missense variants (Arg688Gln, Phe749Ser, and Arg316Gly) are severe loss-of-function alleles, and the other five missense variants (Pro867Ala, Ala343Val, Trp237Cys, Asp507Val, and Arg261Trp) are hypomorphic alleles.

The splicing effect of missense variant p.Val488Val

Individual 3 in family 2 carries compound heterozygous variants (c.2018G>A [p.Arg673Gln]/c.1464T>C [p.Val488Val]). Since the synonymous c.1464T>C [p.Val488Val] variant was predicted to cause splice site changes, we assessed its effect on *OGDHL* transcript. RNA was extracted from fibroblasts of individual 3 and retro-transcribed into cDNA. Despite very low expression of *OGDHL* in this specimen, we were able to amplify a large portion of the *OGDHL* transcript (exons from 5 to 19), which showed a single band in controls and a faint double band in individual 3. By performing NGS, besides the full-length transcript we detected an alternative transcript corresponding to exon 11 skipping, Δ exon 11 (Figures 6B and 6C). Interestingly, the Δ exon 11 transcript is present also in controls, but at low percentages (≈15%) (Figure 6D). Contrariwise, in individual 3, the Δ exon 11 transcript is ≈50%, suggesting that this overrepresentation of the Δ exon 11 transcript is favored by the presence of the synonymous variant.

Defective mitochondrial metabolism in neurons lacking *OGDHL*

To determine whether loss of *dOgdh* in neurons affect Krebs cycle metabolism, we performed metabolite profiling for *Drosophila* larval brains with *dOgdh* ko and control brains by LC/MS. We found that α-KG, the substrate of

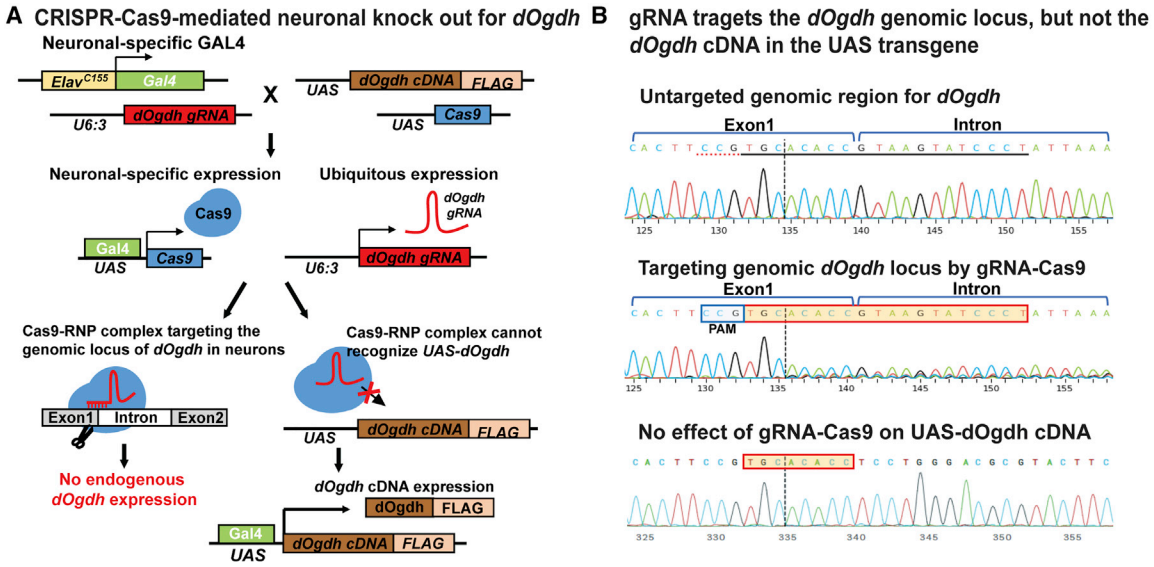

C Lethality rescue for neuronal *dOgdh* ko by expression of *dOgdh* cDNA carrying mutations

	Genotypes	Rescue
elav^{C155}-Gal4 ; U6:3 -gRNA targeting dOgdh ; UAS-Cas9.P2	*UAS-empty*	Lethal
	UAS-dOgdh(WT)-Flag	Viable
	UAS-dOgdh(S793L)-Flag	Lethal
	UAS-dOgdh(P867A)-Flag	Viable
	UAS-dOgdh(R688Q)-Flag	Lethal
	UAS-dOgdh(F749S)-Flag	Lethal
	UAS-dOgdh(A343V)-Flag	Viable
	UAS-dOgdh(W237C)-Flag	Viable
	UAS-dOgdh(D507V)-Flag	Viable
	UAS-dOgdh(R261W)-Flag	Viable
	UAS-dOgdh(R316G)-Flag	Lethal

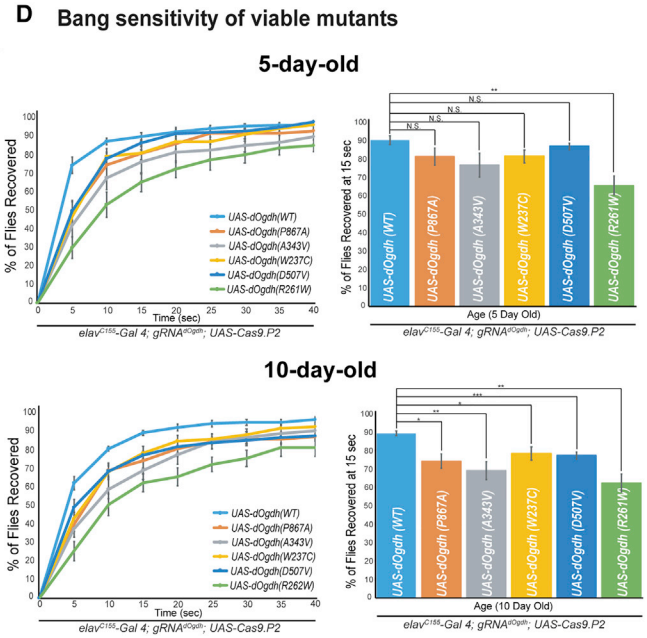

Figure 5. CRISPR-Cas9-mediated neuronal *dOgdh* knockout model shows various strength of *OGDHL* missense variants
(A) Schematic of CRISPR-Cas9-mediated neuron-specific *dOgdh* knockout and cDNA rescue system.
(B) Sanger sequencing from fly heads carrying *elav^{C155}-Gal4*, *U6:3-gRNA^{dOgdh}*, *UAS-Cas9.P2*, together with *UAS-dOgdh^{WT}* showed that the gRNA targets the genomic locus of *dOgdh* but not for the *UAS-dOgdh* transgene.
(C) The lethality caused by neuronal knockout of *dOgdh* was rescued by wild-type *dOgdh* and *dOgdh* carrying Pro867Ala, Ala343Val, Trp237Cys, Asp507Val, and Arg261Trp but not by those carrying Arg688Gln, Phe749Ser, and Arg316Gly.
(D) Flies with neuronal knockout for *dOgdh* expressing Pro867Ala, Ala343Val, Trp237Cys, Asp507Val, or Arg261Trp exhibited progressive defects in recovery from bang stress compared to flies expressing WT *dOgdh*. Six to seven biological replicates (20 flies per genotype) were quantified. Error bars indicate SEM. p values were obtained by the Student's t test. *$p < 0.05$, **$p < 0.01$,***$p < 0.001$. N.S. indicates not statistically significant.

DOGDH, is significantly elevated in the *dOgdh* ko brains (Figure 7A). In contrast, the levels of other Krebs cycle metabolites including citrate, malate, and fumarate are decreased in the *dOgdh* mutant brains compared to those from controls (Figure 7A), indicating that *dOgdh* is required for normal Krebs cycle metabolism in the brains.

We anticipate that *dOgdh* loss in the brain leads to a decrease in the levels of succinate, the product of DOGDH reaction. The levels of succinate in the *dOgdh* mutant brains, however, are comparable to those in controls, suggesting that succinate could be replenished with amino acids, including methionine, isoleucine, valine, and threonine, by anaplerotic reactions.[35] Interestingly, while the levels of threonine, valine, and isoleucine are similar in the mutants and controls, methionine are markedly decreased in the *dOgdh* ko brains (Figure 7B). This suggests

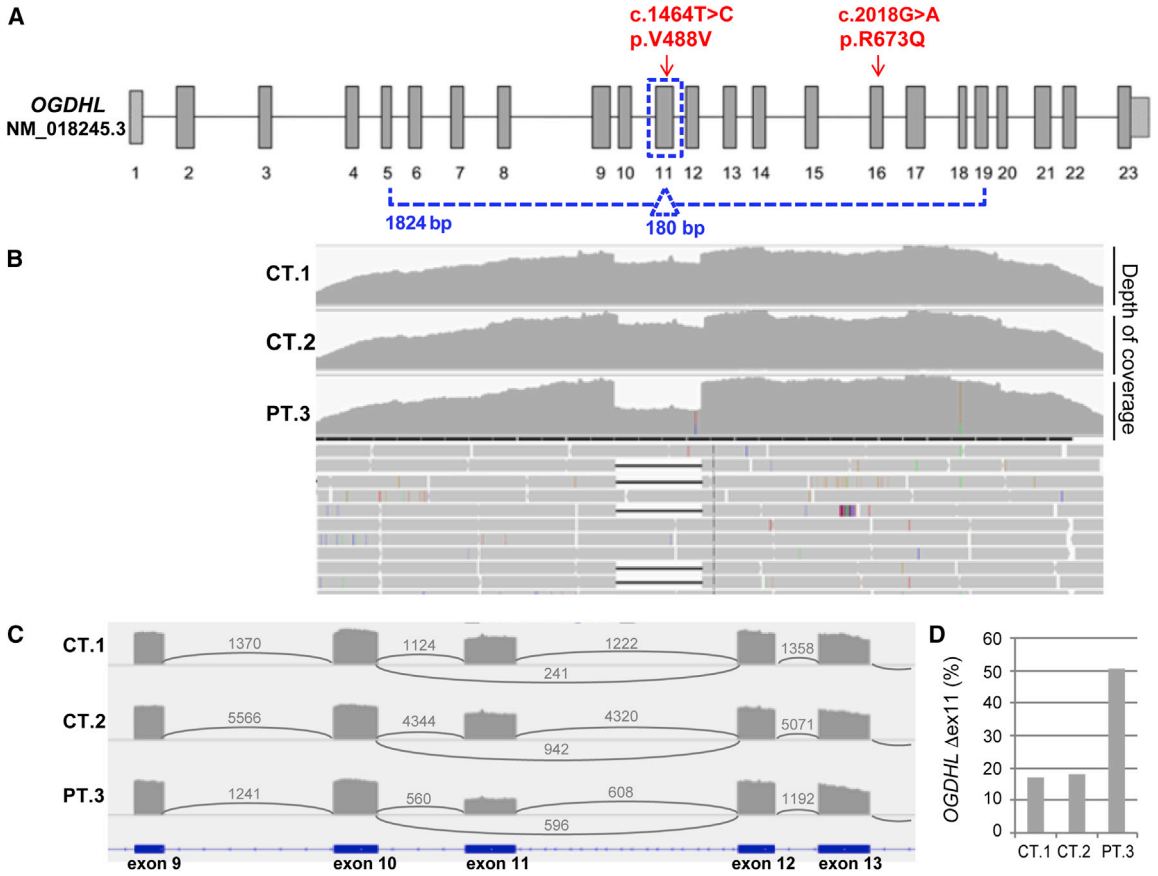

Figure 6. NGS analysis of *OGDHL* transcript for individual 3
(A) Schematic structure of the *OGHDL* transcript (GenBank: NM_152416.3). The arrows indicate the variants identified in individual 3. The dotted line corresponds to the analyzed PCR amplicon (exons from 5 to 19) and highlights the exon 11.
(B) Profiles of depth of coverage obtained through NGS on *OGDHL* transcript PCR products encompassing exons from 5 to 19. RNA was extracted from fibroblasts of individual 3 (PT3) and two control samples (CT1 and CT2). The drop in coverage depth corresponds to the alternative transcript with exon 11 skipping (Δex11).
(C) *OGDHL* Sashimi plot of exon skipping in individual 3's and control fibroblasts. The number of split reads spanning the given intron is indicated on the exon-connecting lines. The involved exons are depicted at the bottom.
(D) Quantification of exon 11 skipping (Δex11). Graphs of the coverage ratio (in percentage) between the *OGDHL* Δex11 isoform and the full-length isoform, calculated for all the samples analyzed by NGS (individual 3, PT3, and two controls, CT1 and CT2).

that methionine catabolism most likely replenishes succinate pools as a compensatory mechanism.

Given that Krebs cycle metabolism is required for mitochondrial respiration, we hypothesize that *OGDHL* loss in human neurons leads to defects in mitochondrial respiration. To test this, we generated SH-SY5Y, human neuroblastoma cell line, with mutations in *OGDHL* by using CRISPR-Cas9-mediated gene editing.[26,27] Lentivirus-mediated transduction of two gRNAs that target *OGDHL* exon 2 caused significant fraction of cells to carry InDel mutations (95% InDels by gRNA1; 98% InDels by gRNA2) (Figure 7C). In contrast, scramble gRNA did not lead to gene editing in *OGDHL* exon 2 (Figure 7C). We confirmed that SH-SY5Y cells carrying mutations in *OGDHL* exhibited a decrease in the protein levels of OGDHL but not OGDH (Figure 7D). We measured oxygen consumption and found that *OGDHL* ko cells had significantly lower oxygen consumption rates (OCRs) as well as ATP production compared to the control cells (Figure 7E), indicating that OGDHL is required for normal mitochondrial respiration and energy production in human neurons. Hence, the critical role of OGDHL in mitochondrial metabolism in neurons suggests that defects in the Krebs cycle and mitochondrial respiration contribute to the etiology of persons carrying bi-allelic variants in *OGDHL*.

Discussion

We previously identified a single individual carrying a recessive variant (p.Ser778Leu) in *OGDHL* with neurodevelopmental phenotypes.[21,30] However, with only a single individual, the causality of this *OGDHL* variant to human disease was not firmly established and the definition of the associated phenotypes was incomplete. Here, we reported nine individuals from eight unrelated families with bi-allelic variants at the *OGDHL* locus primarily presenting with developmental delay accompanied with variable

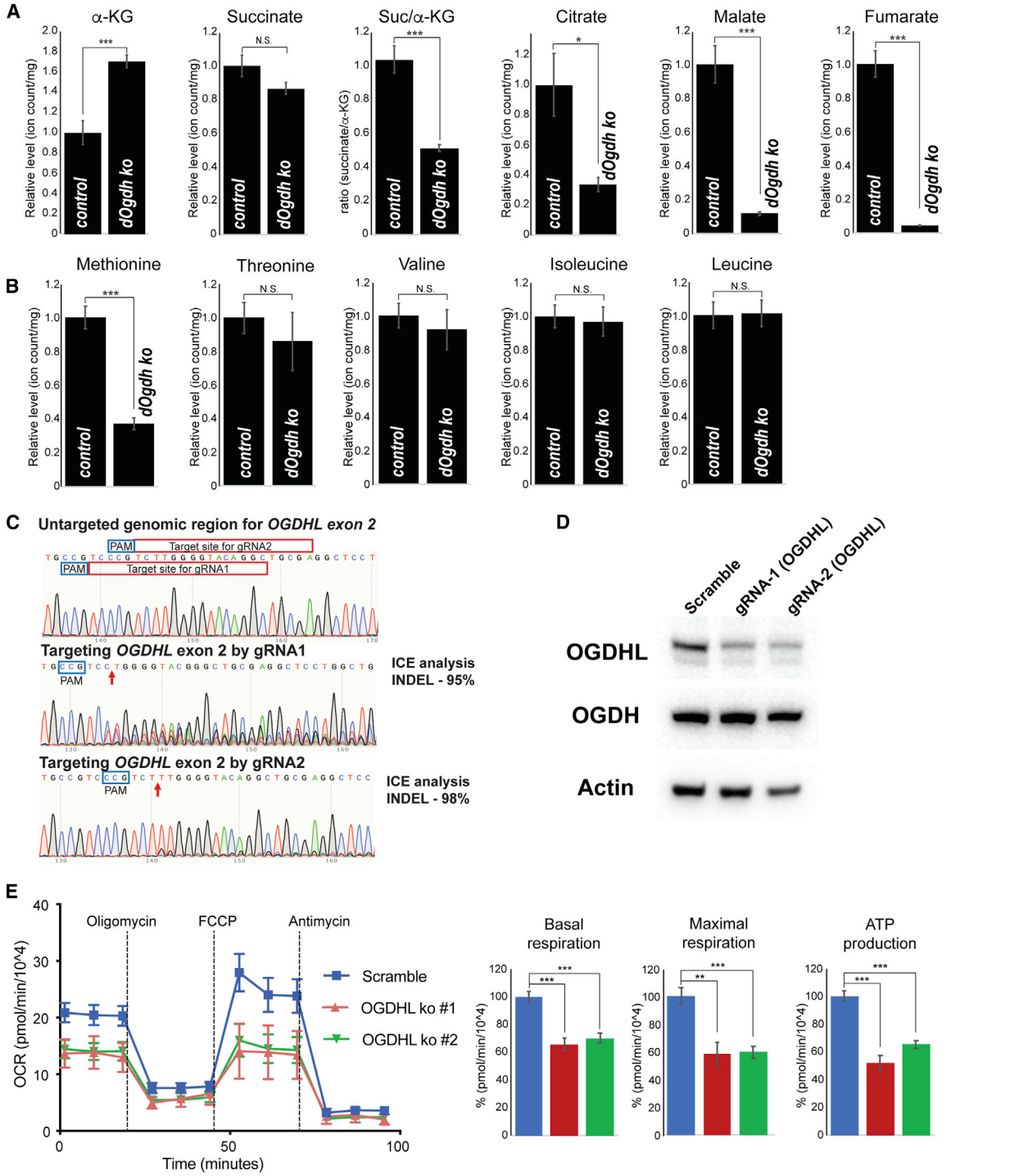

Figure 7. Neurons lacking functional OGDHL leads to defects in mitochondrial metabolism

(A) Relative levels of the indicated Krebs cycle metabolites in larval brains of neuron-specific *dOgdh* knockout (*elav^{C155}-Gal4*, *U6:3-gRNA^{dOgdh}*, *UAS-Cas9.P2*) and controls (*elav^{C155}-Gal4*, *U6:3-gRNA^{dOgdh}*).

(B) Relative levels of the indicated amino acids in larval brains of neuron-specific *dOgdh* knockout (*elav^{C155}-Gal4*, *U6:3-gRNA^{dOgdh}*, *UAS-Cas9.P2*) and controls (*elav^{C155}-Gal4*, *U6:3-gRNA^{dOgdh}*).

(C) Sanger sequencing results for genomic region for exon 2 of *OGDHL* of SH-SY5Y cells with or without gene editing. Target sites of gRNA1 and gRNA2 were highlighted with red box. PAM sites were labeled with blue box. Arrows indicate Cas9 cleavage sites.

(D) Immunoblots for protein levels of OGDHL, OGDH, and Actin in SH-SY5Y cells with or without Cas9-directed gene editing.

(E) Oxygen consumption rate (OCR) of SH-SY5Y cells with or without CRISPR-Cas9-directed editing for *OGDHL*. The cells were treated sequentially (vertical lines) with 1 μM oligomycin, 1 μM FCCP, and 1 μM antimycin A. Quantification of basal respiration, maximal respiration, and ATP production were shown in bar graphs. Error bars indicate SEM. p values were obtained by the Student's t test. *$p < 0.05$, **$p < 0.01$, ***$p < 0.001$. N.S. indicates not statistically significant.

neurological and neurodevelopmental phenotypes. The following evidence supports the causality of the bi-allelic variants in *OGDHL* to the human neurological disease. First, nine individuals in eight unrelated families have been identified in our manuscript with the same consistent genetic defect, derived by independent filtration of WES variants in different neurological centers. Second, all the identified variants are likely to have damaging effects. Indeed, two nonsense variants predict the formation of truncated proteins and a synonymous variant affects splicing. The *Drosophila* models showed that three missense variants are LOF, whereas five missense variants are hypomorphic alleles. Moreover, all eight missense variants hit highly conserved residues of OGDHL. In addition, we would like to stress the fact that all individuals belong to pedigrees compatible with a recessive trait and harbor bi-allelic variants in *OGDHL*, and the deleterious effects of the identified variants have been experimentally proven.

The clinical findings included developmental and epileptic encephalopathy (DEE) defined by early onset seizures and developmental delay, hearing loss, visual impairment, intellectual disability, gait ataxia, and dysmorphic features (Tables 1 and S1). Individual 6 in family 5 presented with hypoplastic corpus callosum and microcephaly (Table S1, Figures 2A and 2E), which are similar to clinical manifestations found in a previously reported single individual carrying a homozygous variant in *OGDHL* (p.Ser778Leu).[21] Several of the clinical features found in our cohort overlap with phenotypes associated with a pathogenic variant in *OGDH* (c.959A>G [p.Asn320Ser]), including gait ataxia, tonic-clonic seizures, and brain atrophy.[12] Pathogenic variants in Krebs cycle genes and other mitochondrial genes, including *AIFM1* (MIM: 300169), also lead to overlapping features found in individuals carrying bi-allelic *OGDHL*.[36–38] Mutations in *MDH2* resulted in DEE (MIM: 154100),[8] while mutations in *DLD*, *SUCLG1*, *SUCLA2*, *SDHA*, and *FH* lead to Leigh syndrome or Leigh-like disease.[1–5]

OGDHL variants p.Arg299Gly (individual 8, family 7), p.Phe734Ser (individual 4, family 3), and p.Arg673Gln (individual 3, family 2) had more deleterious *in silico* prediction scores (CADD > 30, predicted to be the 0.1% most deleterious substitutions in the human genome), which were consistent with the *Drosophila* functional studies demonstrating these three variants as severe LOF alleles (Figure 5C). Importantly, these results were also predicted by the 3D protein structure modeling (Figures 3B and 3C) and the protein level test in *Drosophila* neurons (Figure 3D). Indeed, individual 8, homozygous for p.Arg299Gly, exhibited severe limb and facial muscle weakness and hypotonia as well as severe intellectual disability (Table 1, supplemental notes). On the contrary, the other five missense variants, p.Pro852Ala, p.Ala327Val, p.Trp220Cys, p.Asp491Val, and p.Arg244Trp, had lower CADD prediction scores > 20 (predicted to be the 1% most deleterious substitutions in the human genome) compared to the three severe LOF alleles (CADD > 30) (Table S2). Consistent with the *in silico* prediction, *Drosophila* functional studies demonstrated that these five alleles are hypomorphic (Figures 5C and 5D). Similarly, the synonymous variant p.Val488Val, which had a partial impact on the splicing process, may be considered an hypomorphic allele. Individuals 3 and 4, who carry a combination of severe LOF alleles and mild alleles (individual 3, p.Arg673Gln/p.Val488Val; individual 4, p.Phe734Ser/p.Ala327Val), were the only individuals in our cohort presented with a later disease onset (after 8 and 6 years of life in individuals 3 and 4, respectively) compared to others who presented the disease either at birth or within 6 months of life. A milder phenotype without seizures in individual 3 or drug-controlled epileptic encephalopathy in individual 4 has been reported. The latter has been seizure free and his cognitive functions have recovered in the last 7 years (Table 1, supplemental notes). This suggests that alleles in individuals 3 and 4 are still associated with a residual production of functional protein. The frameshift variant in individual 7 (p.Cys553Leufs*16) and nonsense variant in individual 9 (p.Arg440Ter) lead to early stop codons, which could underlie the cause of disease in early infancy (2–3 months of age), the severe phenotype comprised of visual impairment, bilateral hearing deficit, and seizures in individual 9 as well as the growth retardation and presence of glioma on the brain imaging of individual 7. In families 1 and 5 with functional data suggestive of hypomorphic alleles, we hypothesize that different levels consanguinity in these pedigrees might add difficulty to deduce single disease-causing genes. Overall, the studies on *Drosophila* strongly supported the pathogenicity of the variants, which correlates well with the severity of clinical manifestations in humans.

While *Drosophila* has a single *dOgdh* gene, humans have two paralogs carrying OGDH activity, *OGDHL* and *OGDH*. These two genes appear to have evolved by gene duplication of a single ancestral gene during early vertebrate evolution.[9] Interestingly, it was inferred from a large-scale *Drosophila* genetic screen combined with Mendelian disease study that essential fly genes with two or more human homologs have a higher likelihood of being associated with Mendelian diseases than those that only have a single human homolog because redundant function of duplicated genes may cause genes to be more susceptible to pathogenic mutations.[39] In contrast to ubiquitous *OGDH* expression, brain-specific expression of *OGDHL* suggests that deleterious genetic variants in *OGDHL* result in human disease phenotypes more frequently than those in *OGDH*. Neuronal expression of *OGDHL* also suggests the pivotal role of *OGDHL* in neuronal development and function, which is in agreement with diverse neurodevelopmental phenotypes observed in our cohort of patients. Besides, our analysis of single-cell RNA sequencing results of the cochlear epithelium in several stages of early postnatal mouse development showed that *OGDHL* is expressed in the hair cells, inner pillar cells, and the inner border

cells/inner phalangeal cells (Figure S6).[40,41] These data are consistent with hearing loss found in four individuals of our cohort.

OGDHL is involved in the decarboxylation of α-KG to succinyl-CoA during the Krebs cycle, and its impairment is expected to cause a mitochondrial metabolic defect. Indeed, we found that α-KG is significantly elevated while other Krebs cycle metabolites, including citrate, malate, and fumarate, are decreased in the *dOgdh* ko brains compared to those from controls (Figure 7A). Notably, succinate levels were comparable to controls despite the fact that *dOgdh* loss in the brain should lead to a decrease in the levels of succinate, the product of OGDH and OGDHL reaction. This finding suggests that succinate could be replenished with some amino acids by anaplerotic reactions.[35] While threonine, valine, and isoleucine levels are similar between mutants and controls, methionine levels are significantly decreased in the *dOgdh* ko brains, suggesting succinate is mainly replenished with methionine.

The recessive variant in *OGDH* (GenBank: NM_002541.3; c.959A>G [p.Asn320Ser]) was previously reported to lead to a neurodevelopmental phenotypes[12] similar to those carrying bi-allelic variants in *OGDHL*. The findings suggest that OGDHL in the brain cannot compensate defects of OGDH in spite of their common role in α-KG decarboxylation.[11,13] Why does the brain need both OGDHL and OGDH for its normal development and function? The brain needs sustained energy production obtained from mitochondrial respiration to maintain electrochemical gradients and synaptic transmission, which is essential for development and function of the brain. Hence, it is possible to speculate that both isozymes, OGDHL and OGDH, are required for sustained energy production in neurons in response to a wide-range of α-KG concentration. This idea is supported by the following evidence. First, OGDHL and OGDH in rat brain extract exhibited biphasic substrate saturation kinetics with higher α-KG concentration for full saturation ($K_{m1} = 0.4$ mM) and lower α-KG concentration ($K_{m2} = 0.07$ mM).[13] In contrast, OGDH from heart exhibited a standard Michaelis-Menten kinetics with Km (0.2 mM).[42] Hence, having two isozymes (OGDHL and OGDH) with the two distinct binding affinities ($K_{m1} = 0.4$ mM and $K_{m2} = 0.07$ mM) for the substrate enables the brain to utilize a wide range of α-KG levels for running the Krebs cycle for energy production. Importantly, we showed that *OGDHL* ko human neuronal cells had significantly lower oxygen consumption rates as well as ATP production compared to the control cells (Figure 7E), indicating that both OGDHL and OGDH are required for mitochondrial metabolism in human neurons.

One individual (individual 7 in family 6) exhibited low-grade astrocytoma. In our previous study, we showed that reduction in OGDH activity leads to hyperactive mTORC1 activity in *Drosophila* and mouse embryonic fibroblasts.[21] *OGDHL* silencing was also shown to induce mTORC1 signaling in hepatocellular carcinoma.[43] Interestingly, hyperactivation of mTOR signaling has been associated with other human diseases, including tuberous sclerosis complex-associated subependymal giant cell astrocytomas.[44] mTOR inhibitors have been shown to improve the clinical status of subependymal giant cell astrocytomas and tuberous sclerosis patients.[45] Hence, it is tempting to speculate that treatment with mTOR inhibitors may be a therapeutic avenue for individual 7 with low-grade astrocytoma.

In summary, we have identified nine individuals in eight unrelated families with bi-allelic variants in *OGDHL* showing diverse neurological phenotypes including DEE, visual impairment, hearing loss, intellectual disability, and hypoplastic corpus callosum. Functional study with a novel CRISPR-Cas9-mediated tissue knockout with cDNA rescue system revealed that eight missense *OGDHL* variants are loss-of-function alleles. Further, the analysis of the transcripts from fibroblasts showed that the synonymous variant in family 2 impairs splicing in *OGDHL*. Taken together, we establish *OGDHL* as a disease gene whose impairment leads to a distinct Mendelian mitochondrial disease with mainly neurological phenotypes.

Data and code availability

The variant alleles identified in all families have been deposited on the Leiden Open Variation Database (LOVD) with the following accession numbers: p.Pro852Ala in individual 1 in family 1 (individual ID: 385786; variant ID: 814865); p.Pro852Ala in individual 2 in family 1 (individual ID: 385787; variant ID: 814866); p.Arg673Gln in individual 3 in family 2 (individual ID: 385788; variant ID: 814867); p.Val488Val in individual 3 in family 2 (individual ID: 385788; variant ID: 814868); p.Phe734Ser in individual 4 in family 3 (individual ID: 385790; variant ID: 814869); p.Ala327Val in individual 4 in family 3 (individual ID: 385790; variant ID: 814870); p.Trp220Cys in individual 5 in family 4 (individual ID: 385821; variant ID: 814902); p.Asp491Val in individual 5 in family 4 (individual ID: 385821; variant ID: 814903); p.Arg244Trp in individual 6 in family 5 (individual ID: 385822; variant ID: 814904); p.Cys553Leufs*16 in individual 7 in family 6 (individual ID: 385823; variant ID: 814905); p.Arg299Gly in individual 8 in family 7 (individual ID: 385824; variant ID: 814906); p.Arg440* in individual 9 in family 8 (individual ID: 385825; variant ID: 814907).

Supplemental information

Supplemental information can be found online at https://doi.org/10.1016/j.ajhg.2021.11.003.

Acknowledgments

We thank all individuals and relatives for consent to be part of the study. Families 5–8 were collected as part of the SYNaPS Study Group collaboration funded by The Wellcome Trust and strategic award (Synaptopathies) funding (WT093205 MA and WT104033AIA), and research was conducted as part of the Queen Square Genomics group at University College London, supported by the National Institute for Health Research University College London Hospitals Biomedical Research Centre. We thank former and present Yoon lab members for their input during investigations, particularly Madison Chilian, Yohan Park, David Seo,

and Jae Sun Kang. We thank Holly Van Remmen for her support of Seahorse assays. We thank Scott Plafker for his helpful advices during investigation. We thank Hugo Bellen for his help to initiate this study. We thank the "Cell line and DNA Bank of Genetic Movement Disorders and Mitochondrial Diseases" of the Telethon Network of Genetic Biobanks (grant GTB12001J) and Eurobiobank Network, which supplied biological specimens for family 2. C.L. and D.G. are members of the European Reference Network for Rare Neuromuscular Diseases (ERN EURO-NMD). W.H.Y. is supported by the National Institute of General Medical Sciences (5 P20 GM103636-08) and the National Institute of Neurological Disorders and Stroke (1R01 NS121298-01) of the National Institutes of Health. W.H.Y. was also supported by Presbyterian Health Foundation (PHF 4431-04-04-0 and PHF 4411-05-07-0). H.H. is funded by the MRC (MR/S01165X/1, MR/S005021/1, G0601943), the National Institute for Health Research University College London Hospitals Biomedical Research Centre, Rosetree Trust, Ataxia UK, MSA Trust, Brain Research UK, Sparks GOSH Charity, Muscular Dystrophy UK (MDUK), and Muscular Dystrophy Association (MDA USA). Y.W. was funded by the German Research Foundation (DFG; WE4896/3-1) by the DFG/FNR INTER Research Unit FOR2715 (WE4896/4-1) Treat-ION grant (01GM1907) (continued in supplemental acknowledgments).

Declaration of interests

I.H. serves on the Scientific Advisory Board of Biogen. A.R. is an employee of GeneDx. The remaining authors declare no competing interests.

Received: May 1, 2021
Accepted: October 29, 2021
Published: November 19, 2021

Web resources

GeneDx ClinVar submission page, https://www.ncbi.nlm.nih.gov/clinvar/submitters/26957/
Synthego prediction tools, https://tools.synthego.com/#/

References

1. Grafakou, O., Oexle, K., van den Heuvel, L., Smeets, R., Trijbels, F., Goebel, H.H., Bosshard, N., Superti-Furga, A., Steinmann, B., and Smeitink, J. (2003). Leigh syndrome due to compound heterozygosity of dihydrolipoamide dehydrogenase gene mutations. Description of the first E3 splice site mutation. Eur. J. Pediatr. *162*, 714–718.
2. Ostergaard, E., Schwartz, M., Batbayli, M., Christensen, E., Hjalmarson, O., Kollberg, G., and Holme, E. (2010). A novel missense mutation in SUCLG1 associated with mitochondrial DNA depletion, encephalomyopathic form, with methylmalonic aciduria. Eur. J. Pediatr. *169*, 201–205.
3. Carrozzo, R., Dionisi-Vici, C., Steuerwald, U., Lucioli, S., Deodato, F., Di Giandomenico, S., Bertini, E., Franke, B., Kluijtmans, L.A., Meschini, M.C., et al. (2007). SUCLA2 mutations are associated with mild methylmalonic aciduria, Leigh-like encephalomyopathy, dystonia and deafness. Brain *130*, 862–874.
4. Bourgeron, T., Rustin, P., Chretien, D., Birch-Machin, M., Bourgeois, M., Viegas-Péquignot, E., Munnich, A., and Rötig, A. (1995). Mutation of a nuclear succinate dehydrogenase gene results in mitochondrial respiratory chain deficiency. Nat. Genet. *11*, 144–149.
5. Bourgeron, T., Chretien, D., Poggi-Bach, J., Doonan, S., Rabier, D., Letouzé, P., Munnich, A., Rötig, A., Landrieu, P., and Rustin, P. (1994). Mutation of the fumarase gene in two siblings with progressive encephalopathy and fumarase deficiency. J. Clin. Invest. *93*, 2514–2518.
6. Spiegel, R., Pines, O., Ta-Shma, A., Burak, E., Shaag, A., Halvardson, J., Edvardson, S., Mahajna, M., Zenvirt, S., Saada, A., et al. (2012). Infantile cerebellar-retinal degeneration associated with a mutation in mitochondrial aconitase, ACO2. Am. J. Hum. Genet. *90*, 518–523.
7. Ghezzi, D., Goffrini, P., Uziel, G., Horvath, R., Klopstock, T., Lochmüller, H., D'Adamo, P., Gasparini, P., Strom, T.M., Prokisch, H., et al. (2009). SDHAF1, encoding a LYR complex-II specific assembly factor, is mutated in SDH-defective infantile leukoencephalopathy. Nat. Genet. *41*, 654–656.
8. Ait-El-Mkadem, S., Dayem-Quere, M., Gusic, M., Chaussenot, A., Bannwarth, S., François, B., Genin, E.C., Fragaki, K., Volker-Touw, C.L.M., Vasnier, C., et al. (2017). Mutations in MDH2, Encoding a Krebs Cycle Enzyme, Cause Early-Onset Severe Encephalopathy. Am. J. Hum. Genet. *100*, 151–159.
9. Larsson, T.A., Olsson, F., Sundstrom, G., Lundin, L.G., Brenner, S., Venkatesh, B., and Larhammar, D. (2008). Early vertebrate chromosome duplications and the evolution of the neuropeptide Y receptor gene regions. BMC Evol. Biol. *8*, 184.
10. GTEx Consortium (2013). The Genotype-Tissue Expression (GTEx) project. Nat. Genet. *45*, 580–585.
11. Battle, A., Brown, C.D., Engelhardt, B.E., Montgomery, S.B.; GTEx Consortium; Laboratory, Data Analysis &Coordinating Center (LDACC)—Analysis Working Group; Statistical Methods groups—Analysis Working Group; Enhancing GTEx (eGTEx) groups; NIH Common Fund; and NIH/NCI (2017). Genetic effects on gene expression across human tissues. Nature *550*, 204–213.
12. Yap, Z.Y., Strucinska, K., Matsuzaki, S., Lee, S., Si, Y., Humphries, K., Tarnopolsky, M.A., and Yoon, W.H. (2021). A biallelic pathogenic variant in the OGDH gene results in a neurological disorder with features of a mitochondrial disease. J. Inherit. Metab. Dis. *44*, 388–400.
13. Bunik, V., Kaehne, T., Degtyarev, D., Shcherbakova, T., and Reiser, G. (2008). Novel isoenzyme of 2-oxoglutarate dehydrogenase is identified in brain, but not in heart. FEBS J. *275*, 4990–5006.
14. Legati, A., Reyes, A., Nasca, A., Invernizzi, F., Lamantea, E., Tiranti, V., Garavaglia, B., Lamperti, C., Ardissone, A., Moroni, I., et al. (2016). New genes and pathomechanisms in mitochondrial disorders unraveled by NGS technologies. Biochim. Biophys. Acta *1857*, 1326–1335.
15. Helbig, I., Lopez-Hernandez, T., Shor, O., Galer, P., Ganesan, S., Pendziwiat, M., Rademacher, A., Ellis, C.A., Hümpfer, N., Schwarz, N., et al. (2019). A Recurrent Missense Variant in AP2M1 Impairs Clathrin-Mediated Endocytosis and Causes Developmental and Epileptic Encephalopathy. Am. J. Hum. Genet. *104*, 1060–1072.
16. Retterer, K., Juusola, J., Cho, M.T., Vitazka, P., Millan, F., Gibellini, F., Vertino-Bell, A., Smaoui, N., Neidich, J., Monaghan, K.G., et al. (2016). Clinical application of whole-exome sequencing across clinical indications. Genet. Med. *18*, 696–704.
17. Makrythanasis, P., Maroofian, R., Stray-Pedersen, A., Musaev, D., Zaki, M.S., Mahmoud, I.G., Selim, L., Elbadawy, A.,

Jhangiani, S.N., Coban Akdemir, Z.H., et al. (2018). Biallelic variants in KIF14 cause intellectual disability with microcephaly. Eur. J. Hum. Genet. *26*, 330–339.
18. Mencacci, N.E., Kamsteeg, E.J., Nakashima, K., R'Bibo, L., Lynch, D.S., Balint, B., Willemsen, M.A., Adams, M.E., Wiethoff, S., Suzuki, K., et al. (2016). De Novo Mutations in PDE10A Cause Childhood-Onset Chorea with Bilateral Striatal Lesions. Am. J. Hum. Genet. *98*, 763–771.
19. Perenthaler, E., Nikoncuk, A., Yousefi, S., Berdowski, W.M., Alsagob, M., Capo, I., van der Linde, H.C., van den Berg, P., Jacobs, E.H., Putar, D., et al. (2020). Loss of UGP2 in brain leads to a severe epileptic encephalopathy, emphasizing that biallelic isoform-specific start-loss mutations of essential genes can cause genetic diseases. Acta Neuropathol. *139*, 415–442.
20. Sali, A., and Blundell, T.L. (1993). Comparative protein modelling by satisfaction of spatial restraints. J. Mol. Biol. *234*, 779–815.
21. Yoon, W.H., Sandoval, H., Nagarkar-Jaiswal, S., Jaiswal, M., Yamamoto, S., Haelterman, N.A., Putluri, N., Putluri, V., Sreekumar, A., Tos, T., et al. (2017). Loss of Nardilysin, a Mitochondrial Co-chaperone for α-Ketoglutarate Dehydrogenase, Promotes mTORC1 Activation and Neurodegeneration. Neuron *93*, 115–131.
22. Venken, K.J., He, Y., Hoskins, R.A., and Bellen, H.J. (2006). P [acman]: a BAC transgenic platform for targeted insertion of large DNA fragments in D. melanogaster. Science *314*, 1747–1751.
23. Bischof, J., Maeda, R.K., Hediger, M., Karch, F., and Basler, K. (2007). An optimized transgenesis system for Drosophila using germ-line-specific phiC31 integrases. Proc. Natl. Acad. Sci. USA *104*, 3312–3317.
24. Howlett, I.C., and Tanouye, M.A. (2013). Seizure-sensitivity in Drosophila is ameliorated by dorsal vessel injection of the antiepileptic drug valproate. J. Neurogenet. *27*, 143–150.
25. Ganetzky, B., and Wu, C.F. (1982). Indirect Suppression Involving Behavioral Mutants with Altered Nerve Excitability in DROSOPHILA MELANOGASTER. Genetics *100*, 597–614.
26. Shalem, O., Sanjana, N.E., Hartenian, E., Shi, X., Scott, D.A., Mikkelson, T., Heckl, D., Ebert, B.L., Root, D.E., Doench, J.G., and Zhang, F. (2014). Genome-scale CRISPR-Cas9 knockout screening in human cells. Science *343*, 84–87.
27. Sanjana, N.E., Shalem, O., and Zhang, F. (2014). Improved vectors and genome-wide libraries for CRISPR screening. Nat. Methods *11*, 783–784.
28. Sobreira, N., Schiettecatte, F., Boehm, C., Valle, D., and Hamosh, A. (2015). New tools for Mendelian disease gene identification: PhenoDB variant analysis module; and GeneMatcher, a web-based tool for linking investigators with an interest in the same gene. Hum. Mutat. *36*, 425–431.
29. Sobreira, N., Schiettecatte, F., Valle, D., and Hamosh, A. (2015). GeneMatcher: a matching tool for connecting investigators with an interest in the same gene. Hum. Mutat. *36*, 928–930.
30. Karaca, E., Harel, T., Pehlivan, D., Jhangiani, S.N., Gambin, T., Coban Akdemir, Z., Gonzaga-Jauregui, C., Erdin, S., Bayram, Y., Campbell, I.M., et al. (2015). Genes that Affect Brain Structure and Function Identified by Rare Variant Analyses of Mendelian Neurologic Disease. Neuron *88*, 499–513.
31. Sherrill, J.D., Kc, K., Wang, X., Wen, T., Chamberlin, A., Stucke, E.M., Collins, M.H., Abonia, J.P., Peng, Y., Wu, Q., et al. (2018). Whole-exome sequencing uncovers oxidoreductases DHTKD1 and OGDHL as linkers between mitochondrial dysfunction and eosinophilic esophagitis. JCI Insight *3*, e99922.
32. Venken, K.J., Schulze, K.L., Haelterman, N.A., Pan, H., He, Y., Evans-Holm, M., Carlson, J.W., Levis, R.W., Spradling, A.C., Hoskins, R.A., and Bellen, H.J. (2011). MiMIC: a highly versatile transposon insertion resource for engineering Drosophila melanogaster genes. Nat. Methods *8*, 737–743.
33. Diao, F., Ironfield, H., Luan, H., Diao, F., Shropshire, W.C., Ewer, J., Marr, E., Potter, C.J., Landgraf, M., and White, B.H. (2015). Plug-and-play genetic access to drosophila cell types using exchangeable exon cassettes. Cell Rep. *10*, 1410–1421.
34. Port, F., Chen, H.M., Lee, T., and Bullock, S.L. (2014). Optimized CRISPR/Cas tools for efficient germline and somatic genome engineering in Drosophila. Proc. Natl. Acad. Sci. USA *111*, E2967–E2976.
35. Owen, O.E., Kalhan, S.C., and Hanson, R.W. (2002). The key role of anaplerosis and cataplerosis for citric acid cycle function. J. Biol. Chem. *277*, 30409–30412.
36. Ghezzi, D., Sevrioukova, I., Invernizzi, F., Lamperti, C., Mora, M., D'Adamo, P., Novara, F., Zuffardi, O., Uziel, G., and Zeviani, M. (2010). Severe X-linked mitochondrial encephalomyopathy associated with a mutation in apoptosis-inducing factor. Am. J. Hum. Genet. *86*, 639–649.
37. Rinaldi, C., Grunseich, C., Sevrioukova, I.F., Schindler, A., Horkayne-Szakaly, I., Lamperti, C., Landouré, G., Kennerson, M.L., Burnett, B.G., Bönnemann, C., et al. (2012). Cowchock syndrome is associated with a mutation in apoptosis-inducing factor. Am. J. Hum. Genet. *91*, 1095–1102.
38. Zong, L., Guan, J., Ealy, M., Zhang, Q., Wang, D., Wang, H., Zhao, Y., Shen, Z., Campbell, C.A., Wang, F., et al. (2015). Mutations in apoptosis-inducing factor cause X-linked recessive auditory neuropathy spectrum disorder. J. Med. Genet. *52*, 523–531.
39. Yamamoto, S., Jaiswal, M., Charng, W.L., Gambin, T., Karaca, E., Mirzaa, G., Wiszniewski, W., Sandoval, H., Haelterman, N.A., Xiong, B., et al. (2014). A drosophila genetic resource of mutants to study mechanisms underlying human genetic diseases. Cell *159*, 200–214.
40. Kolla, L., Kelly, M.C., Mann, Z.F., Anaya-Rocha, A., Ellis, K., Lemons, A., Palermo, A.T., So, K.S., Mays, J.C., Orvis, J., et al. (2020). Characterization of the development of the mouse cochlear epithelium at the single cell level. Nat. Commun. *11*, 2389.
41. Kubota, M., Scheibinger, M., Jan, T.A., and Heller, S. (2021). Greater epithelial ridge cells are the principal organoid-forming progenitors of the mouse cochlea. Cell Rep. *34*, 108646.
42. McMinn, C.L., and Ottaway, J.H. (1977). Studies on the mechanism and kinetics of the 2-oxoglutarate dehydrogenase system from pig heart. Biochem. J. *161*, 569–581.
43. Dai, W., Xu, L., Yu, X., Zhang, G., Guo, H., Liu, H., Song, G., Weng, S., Dong, L., Zhu, J., et al. (2020). OGDHL silencing promotes hepatocellular carcinoma by reprogramming glutamine metabolism. J. Hepatol. *72*, 909–923.
44. Franz, D.N., Belousova, E., Sparagana, S., Bebin, E.M., Frost, M., Kuperman, R., Witt, O., Kohrman, M.H., Flamini, J.R., Wu, J.Y., et al. (2013). Efficacy and safety of everolimus for subependymal giant cell astrocytomas associated with tuberous sclerosis complex (EXIST-1): a multicentre, randomised, placebo-controlled phase 3 trial. Lancet *381*, 125–132.
45. Ebrahimi-Fakhari, D., and Franz, D.N. (2020). Pharmacological treatment strategies for subependymal giant cell astrocytoma (SEGA). Expert Opin. Pharmacother. *21*, 1329–1336.